Geology of Ore Deposits, Vol. 45, No. 3, 2003, pp. 171–200. Translated from Geologiya Rudnykh Mestorozhdenii, Vol. 45, No. 3, 2003, pp. 195–227.

Mineralogy, Geochemistry, and Genesis of Gold–Sulfide–Selenide–Telluride Ores from the Kairagach Deposit (Uzbekistan)

V. A. Kovalenker*, [1], O. Yu. Plotinskaya*, V. Yu. Prokof'ev*, Yu. L. Gertman, R. I. Koneev***, and V. V. Pomortsev****

**Institute of Geology of Ore Deposits, Petrography, Mineralogy, and Geochemistry, Russian Academy of Sciences, Staromonetnyi per. 35, Moscow, 119017 Russia*

***State Geological Enterprise Tashkentgeologiya, ul. Akhunbabaeva 21, Eshonguzar Settlement, 702050 Uzbekistan*

****Ulugbek National University, Vuzgorodok, Tashkent, 700095 Uzbekistan*

Received December 16, 2002

Abstract—The Late Paleozoic Kairagach epithermal gold deposit belongs to the high-sulfidation (acid–sulfate) type. It is located at the northern slope of the Kuramin Ridge in the central Tien Shan, 3.5 km northwest of the Kochbulak deposit, being confined to the volcanic andesite–dacite sequence (C_{2-3}) composing the northeastern segment of the Karatash caldera. Volcanogenic sequences are intruded by subvolcanic dacite–porphyry and diorite–porphyry intrusions, as well as granodiorite–porphyry and porphyritic diabase dikes of the northeastern strike. The gold–sulfide–selenide–telluride mineralization of the Diabazovaya zone, which encloses the main gold resources, associates with these dikes. Unlike typical epithermal deposits of the high-sulfidation type with Au–Cu geochemical specialization of ores, the Kairagach deposit is characterized by distinct Au–Sn–Bi–Se–Te mineralization, which includes over 80 ore minerals, including new and rare ones. This paper discusses data on the geological structure of the deposit, ore geochemistry, variations in chemical composition, mode of occurrence and parageneses of native elements (Au, Ag, Te, Sn, Bi); sulfides of Fe, Cu, Pb, Zn, and Ag; fahlores of the tetrahedrite–tennantite–annivite–goldfieldite series; bismuthinite–aikinite, junoite, and pavonite sulfosalts; Cu and Fe sulfostannate; various Au, Ag, Pb, Fe, Hg, Bi, and Sb tellurides and Bi sulfoselenides; and Fe and Sn oxides. The chemical composition of ordinary, high-grade, and bonanza ores and the vertical and lateral (including hidden) mineralization zoning, as well as the succession of mineral parageneses, *P–T* parameters, composition of mineral-forming fluids, and main factors and mechanisms responsible for the formation of gold-productive mineral associations, are considered. The variations in the S, C, O, and H compositions of ore minerals are used to define probable sources of water and ore components in ore-forming fluids. The results of thermodynamic modeling of probable gold occurrence and transportation in the mineral-forming solution are also discussed.

INTRODUCTION

In recent publications, epithermal deposits are usually subdivided into two main genetic types—acid–sulfate, or high-sulfidation (HS), and adular–sericite, or low-sulfidation (LS), which differ in the oxidizability and acidity of hydrothermal mineral-forming solutions (Heald *et al.*, 1987; White and Hedenquist, 1990). Oxidized acid and reduced almost neutral fluids are characteristic of the former and latter solutions, respectively. The gold–telluride epithermal deposits are closely related to magmatism with elevated alkalinity and characterized by peculiar geochemical (Te–V–F) and mineral (tellurides, fluorite, roscoelite, vanadium-bearing sulfides) associations. Thus, some researchers relate them to the gold–telluride or "alkalic" A-type (Bonham, 1986; Richards, 1995), which can be referred to the low-sulfidation type.

Although the Late Paleozoic Kairagach epithermal gold ore deposit is characterized by relatively low mineral reserves, estimated to equal 50 t of Au and 150 t of Ag (Islamov *et al.*, 1999), it is of significant importance for the study of epithermal ore genesis. The deposit is located in immediate proximity to the well-known Kochbulak gold–telluride deposit, bearing features peculiar to all the above-mentioned types of epithermal mineralization (Kovalenker *et al.*, 1997). Nevertheless, despite the fact that both these deposits are Late Paleozoic in age, localized within a single volcanic structure, and presumably produced by a single ore-forming system, they show notable differences. Dissimilar to the Kochbulak deposit, where ores occur mainly within veins filling fractures and in hydrothermal breccias, in the Kairagach deposit, zones of the veinlet–disseminated mineralization are clearly controlled by systems of diabase–porphyry dikes. In addition, ores from the Kairagach deposit are characterized by the higher role of selenide mineralization and sulfates (barite and

[1]Corresponding author: V.A. Kovalenker. E-mail: vak@igem.ru

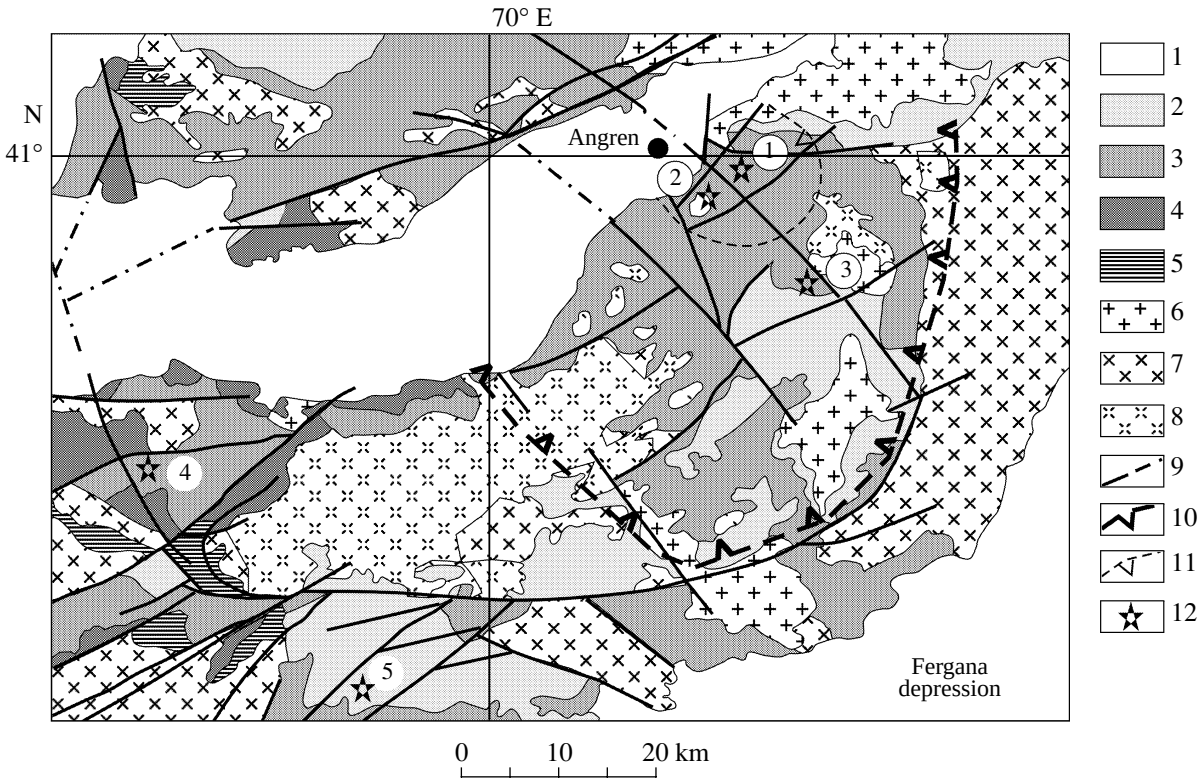

Fig. 1. Schematic geological map of the central part of the Kuramin Ridge. (1) Mesozoic–Cenozoic rocks; (2) rhyolite formation (C_3–P_1); (3) Andesite–dacite formation (C_{2-3}); (4) volcanogenic–sedimentary rocks (D_1–C); (5) Upper Paleozoic metamorphosed rocks (O_3–S); (6–8) igneous rocks: (6) prebatholithic complex (γPZ_2), (7) granitoids of the Karamazar complex (γC_2), and (8) ore-bearing porphyric plutons ($\gamma\delta\pi C_3$–P_1); (9) faults; (10) contour of the Lashkerek syneclise; (11) contour of the Karatash (Kochbulak) caldera; (12) deposits: (1) Kairagach, (2) Kochbulak, (3) Lashkerek, (4) Almalyk, and (5) Kanimansur.

anhydrite), as well as by insignificant development of incrustate and rhythmically banded textures of vein filling, as compared with Kochbulak ores.

Because of the peculiar and complex composition of ores from the Kairagach deposit, which include over 80 ore minerals (native elements, sulfides, sulfosalts, selenides, tellurides, oxides), the main focus at early stages of ore study was on their mineralogy. These investigations resulted in discovery of several rare, including new, minerals (Badalov and Spiridonov, 1983; Badalov *et al.*, 1984; Kovalenker, 1986; Kovalenker and Heinke, 1984; Kovalenker *et al.*, 1979, 1984, 1986, 1987; Spiridonov and Badalov, 1983; Spiridonov *et al.*, 1983).

Recently, Kairagach ores were studied using methods of paragenetic analysis, thermocryometry of fluid inclusions, isotopic geochemistry, and thermodynamic modeling. The results of these studies have been partly published (Plotinskaya and Kovalenker, 1998; Plotinskaya *et al.*, 1998, 2001), but the genesis of Kairagach ores, unique in their mineral composition, remains unclear. In this paper, we summarize the available data on the geological structure, mineralogy, and geochemistry of the ores; the distribution of stable isotopes in sulfides and vein minerals; the *PT* parameters; the gas, anion, and isotopic composition of mineral-forming solutions; gold occurrence modes; and sources of water and ore-forming components.

GEOLOGICAL POSITION AND GENERAL DESCRIPTION OF THE KAIRAGACH DEPOSIT

The Kairagach deposit is located at the northern slope of the Kuramin Ridge of the Central Tien Shan (Republic of Uzbekistan) near the town of Angren (Fig. 1). The geological position of the deposit is controlled by its location within the Karatash (Kochbulak, after Tulyaganov *et al.*, 1984) caldera in the northern part of the Lashkerek syncline at the intersection of the South Angren and Lashkerek–Dukent zones of concealed faults (Islamov *et al.*, 1999). The gold–copper–porphyry and epithermal gold deposits of the Almalyk ore district, as well as the uranium (Mailikatan), silver–tin–polymetallic, and fluorite deposits of the Naugarzan ore district, are associated with the South Angren fault zone, whereas silver–polymetallic (Lashkerek), gold–silver (Kyzylalmai ore field) and uranium (Alatan'ga, Dzhekindek) deposits are associated with the Lashkerek–Dukent zone.

The Kairagach deposit is localized within a slightly elongated (in the north–south direction) northeastern segment (5 × 7 km) of the Karatash caldera, 3.5 km

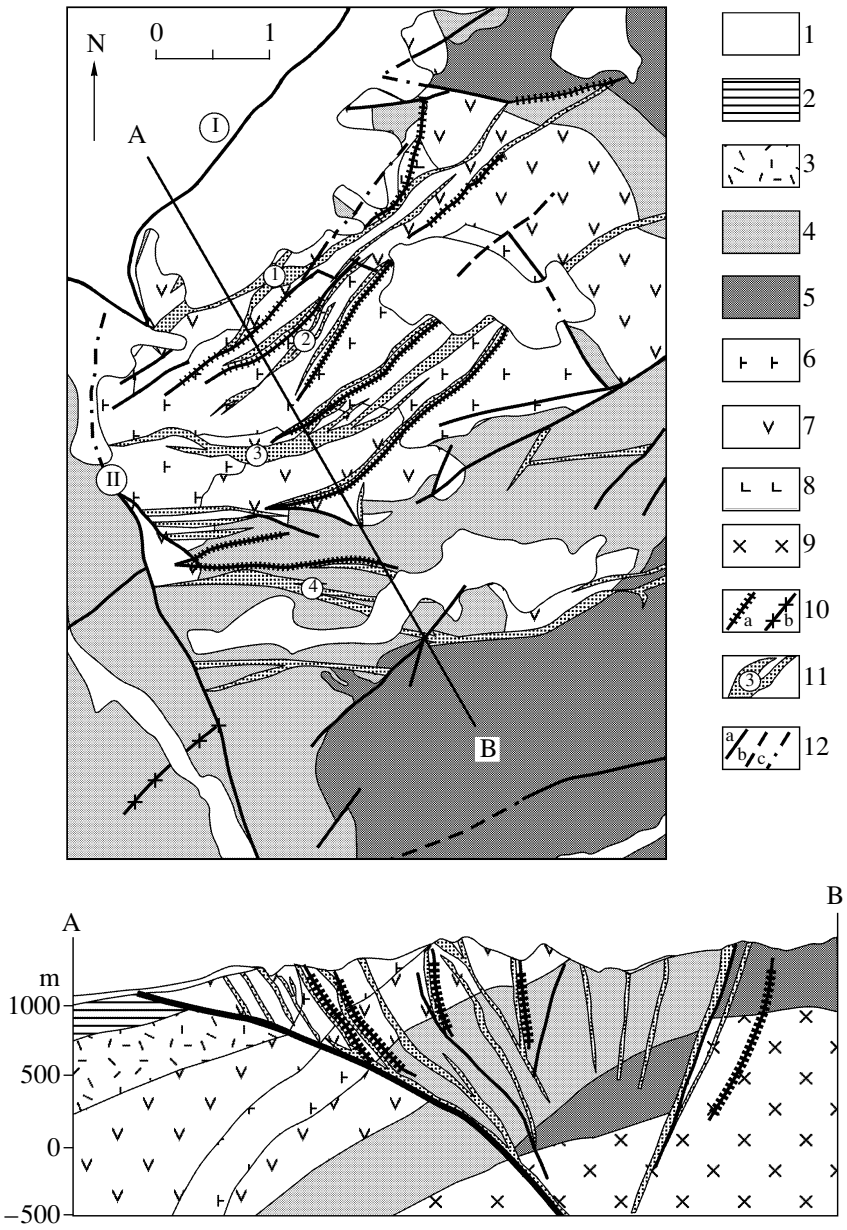

Fig. 2. Schematic geological map of the Kairagach deposit and cross section along line A–B: (1) sand, sandstone, limestone (KZ); (2) clay, siltstone, sandstone, coal (J_{1-2}); (3) rhyolite formation (C_3); (4)–(7) andesite–dacite formation (C_{2-3}); (4) andesitic and andesite–dacite tuffs and lavas (C_{2-3}nd); (5) porphyritic trachyandesite (C_{2-3}ak); (6) subvolcanic porphyritic andesite bodies; (7) subvolcanic dacite–porphyry bodies; (8) syenite–porphyries ($\xi\delta\mu C_{2-3}$); (9) granodiorites ($\gamma\delta C_{2-3}$); (10) porphyritic diabase ($\beta\mu C_3$–P_1) (a) and granodiorite ($\gamma\delta C_{2-3}$) (b) dikes; (11) tectonic dislocations: proven (a), hypothetical (b), and hidden under Mesozoic–Cenozoic sediments (c): (I) Angren (Shagauz) thrust and (II) Karatash fault.

northeast of the large Kochbulak epithermal gold–telluride deposit (Kovalenker *et al.*, 1997), which is confined to the southwestern segment of this volcanic structure. Some researchers consider the Kochbulak and Kairagach deposits as elements of a single Kochbulak ore field confined to the Karatash caldera. The boundary between these deposits coincides with the Karatash fault. On the northwest, the Kairagach deposit is bounded by the Angren (Akhangaran) fault, which corresponds to the Angren graben, filled with Mesozoic coal-bearing sequences, and on the south, by large northeast-oriented faults (Fig. 2).

The Karatash caldera is composed of andesites and dacites (lavas and pyroclastic rocks) of the Akcha (C_2) and Nadak ($C_{2,2-3}$) suites, rhyolites (lavas and pyroclastic rocks) of the Oyasai and Kyzylnura (C_3–P_1) suites, and subvolcanic bodies (Fig. 2). The total thickness of volcanogenic rocks amounts to 1.0–1.5 km. On flanks

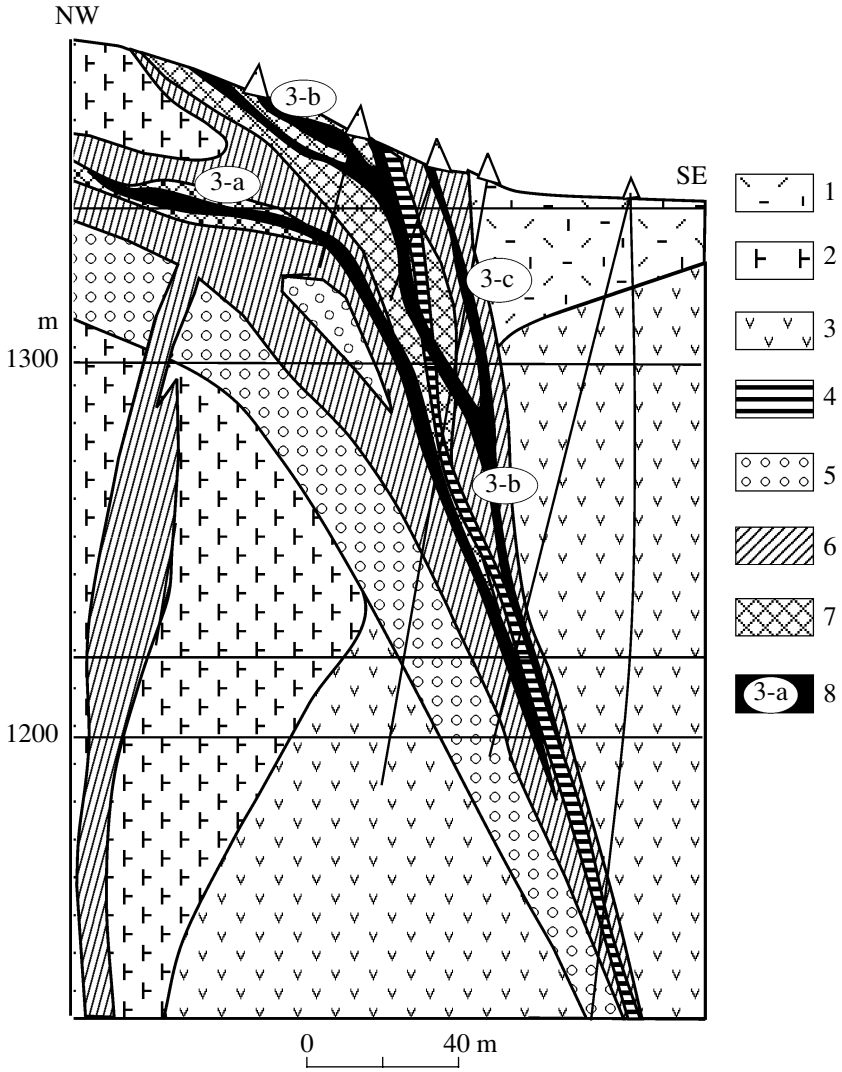

Fig. 3. Geological cross section of the Diabazovaya zone: (1–3) andesite–dacite formation: (1) andesitic, andesite–dacitic, and dacitic tuffs, (2) porphyritic andesite and andesite–dacite, and (3) porphyritic andesite and basaltic andesite; (4) dikes of porphyritic diabase; (5) zones of quartz–carbonate–sericite alterations; (6) zones of metasomatic silicification; (7) zones of quartz and quartz–barite veins; (8) ore bodies.

of the structure, beds dip gently toward its center at angles of 30°–35°. In chemical composition, the rocks are intermediate between calc–alkaline and subalkaline high-potassic varieties of the latite group (Islamov *et al.*, 1999).

In the central part of the caldera, effusive–pyroclastic rocks of the Nadak suite are intruded by a stock-shaped subvolcanic body of porphyritic trachyandesite 1.2×3 km in size, the northern endocontact part of which hosts ore-bearing zones of the Kairagach deposit (Fig. 2).

The main ore-enclosing rocks of the Kairagach deposit are volcanics of the Nadak suite composed of lithoclastic andesite and andesite–dacite tuffs alternating with porphyritic andesite lavas. They are intruded by a system of younger subvolcanic bodies of dacite–porphyry (with large feldspar phenocrysts) and diorite–porphyry. Abundant diabase–porphyry dikes of the northeastern strike occur throughout the deposit and granodiorite–porphyry dikes are developed in its eastern and southeastern parts. According to geophysical data, the deposit presumably encloses subsurface hypabyssal granodiorite bodies (Fig. 2).

The trachyandesite–porphyry subvolcanic body is rimmed by zones of intense rock alteration from 5 to 500 m wide. Most widespread are albite–chlorite, chlorite–carbonate, sericite–chlorite, and sericite–carbonate metosomatites of the propilitic facies, which are subjected to pre-ore and wall rock alterations. The pre-ore rocks are mostly represented by monoquartzites, frequently containing diaspore (similarly to the Kochbulak deposit) and usually developed along contacts of diabase dikes, and pyrophyllite–diaspore–kaolinite–alunite rocks of the advanced argillisite type (secondary

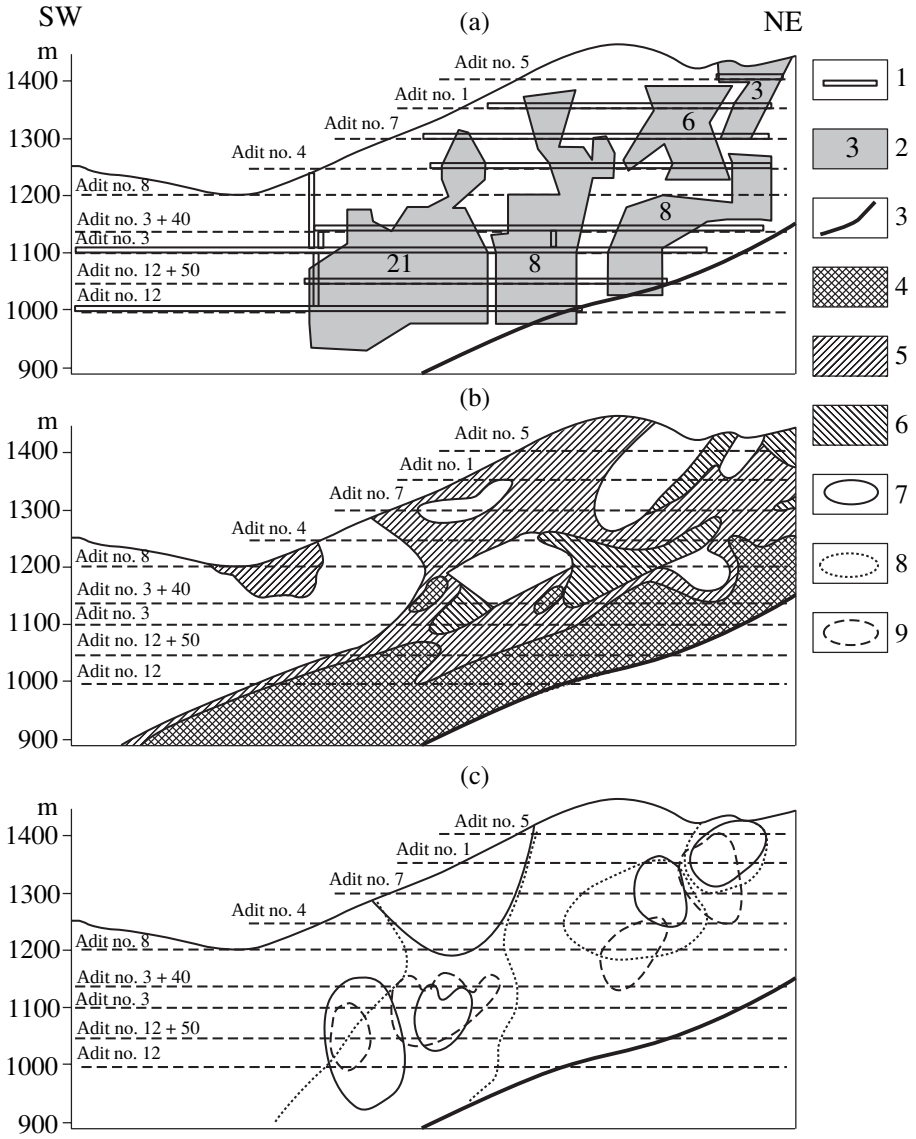

Fig. 4. Distribution of ore bodies (a), ore types (b), and contents of main useful components (c) within the Diabazovaya zone. Longitudinal projection on the vertical plane. (1) Underground workings; (2) commercial ore bodies; (3) Angren thrust; (4) high-grade gold-bearing ores (Au/Ag > 1); (5) ordinary Au–Ag ores (Au/Ag = 1.0–0.1); (6) Au–Ag ores (Au/Ag < 0.1); (7) Te content >10 g/t; (8) Se content >10 g/t; (9) Bi content > 200 g/t.

quartzites). The latter rocks contain primarily the kaolinite–alunite association at upper levels, supplemented by diaspore and pyrophyllite in the lower part of the section. The quartzites overlie spaciously developed quartz–carbonate–sericite–pyrite beresite-like rocks with narrow zones of feldspathization. The rocks almost lack vertical zoning, except for the sericite hydration degree that increases from lower (micas with d = 10.1–10.4 Å) to upper (d = 10.5–10.8 Å) levels, where sericite associates with kaolinite. On the basis of geological relationships, we consider the pyrophyllite–diaspore–kaolinite–alunite rocks as a screening horizon that existed prior to the intrusion of diabase dikes, formation of beresite-like rocks, and ore mineralization. The latter was accompanied by deposition of sericite and hydromicas, mainly of the relatively low-temperature modification 1M, whose degree of hydration also increases upward along the section.

Four elongated (3–5 km) silicification zones with ore mineralization (Diabazovaya, Pervaya, Chukurkotanskaya, and Bedrengetskaya) are controlled by northeast-oriented faults (Fig. 2). Economic mineralization has been discovered in the Diabazovaya and Pervaya zones, which are considered at present to represent the Kairagach deposit proper. These zones are located in the northern contact zone of the subvolcanic trachyandesite–porphyry stock in immediate proximity to each other and subparallel to diabase–porphyry dikes.

The *Diabazovaya zone* is the richest and best-studied ore-bearing zone, of eastern (50°) strike and south-

Table 1. Contents of some ore-forming elements (g/t) and their ratios in balance-off and balance ores

Element	Noncommercial ores in metasomatites									Commercial ores							
										low-grade		high-grade				bonanza	
	6103	6105	6764	6784	6786	6822	6833	7065	7067	6821	7066	6104	6801	6832	6787	6783	6806
Au	0.2	1.0	2.6	2.2	0.2	0.4	0.6	0.4	1.0	4.0	9.0	16.4	20.4	15.2	76.4	129.4	115.8
Ag	0.8	N.d.	8.4	2.6	1.8	5.2	3.8	1.8	2.0	50.0	4.4	4.0	11.2	21.1	10.7	24.4	62.4
Ag/Au	4.0		3.2	1.2	9.0	13.0	5.7	4.5	2.0	12.5	0.5	0.24	0.55	1.4	0.14	0.2	0.5
Se	0.5	0.5	9.7	5.8	5.8	5.6	12.0	4.6	7.2	14.0	7.2	8.8	12.0	28.0	41.0	46.0	110.0
Te	2.0	2.0	2.0	3.0	2.0	4.0	6.0	2.0	4.0	36.0	4.0	11.0	2.0	64.0	120.0	180.0	308.0
Te/Se	4.0	4.0	0.2	0.5	0.3	0.7	0.5	0.4	0.55	2.6	0.55	1.25	0.2	2.3	2.9	3.9	2.8

Note: 6103, 6105, etc., are assay numbers. Au and Ag were determined using the method of assay analysis; Se and Te, by the atomic absorption method at the Central Chemical Laboratory of the State Geological Enterprise "Sharkii Uzbekistan," Tashkent.

eastern dip (angles from 10° to 75°–80°) and enclosing most explored reserves. The axial part of the zone is represented by an intricate system of upward-dichotomizing quartz, quartz–barite, and barite veins and lenticular, stringer-shaped, and breccia bodies with nest, disseminated, and stringer–disseminated ore mineralization that are closely associated with diabase–porphyry dikes 0.5–15 m thick (Fig. 3). Enclosing volcanics and porphyritic diabases are intensely silicified, sericitized, and pyritized. In contact with ore mineralization, altered porphyritic diabases are frequently characterized by elevated contents of Au, Ag, and other metals, which may indicate the pre-ore age of dikes. Figure 3 shows that steeply dipping veins, stringers, silicification zones, and diabase–porphyry dikes change in the upper part of the Diabazovaya zone into a system of low-angle mineralized structures. The total thickness of the zone is 10–40 m in the lower part of the deposit and 60–80 m in its upper portion (Fig. 3).

Several low-angle and steeply dipping (3, 6, 8, 21) ore bodies with economic Au contents have been revealed in this zone (Fig. 4a). In the vertical longitudinal projection, these bodies represent mushroom-shaped ore shoots with economic Au contents increasing to the southwest toward the Karatash fault. At a depth of 300–400 m, mineralization is restricted by the zone of the Shaugaz (or Angren) alpine thrust and the so-called Ogranichivayushchii ("Limiting") fault. Vein-shaped ore bodies are characterized by pinching and swelling (Fig. 3). At present, ore bodies of the Diabazovaya zone are penetrated by adits at eight levels and by exploration boreholes at a vertical interval of 500 m (absolute mark of approximately 1450 m) to 1000 m in adit 12 (Fig. 4a). The intensity of ore mineralization in this zone increases in transition areas from a low-angle (15°–25°) to steeply dipping attitude of the zone (Kovalenker and Heinke, 1984). Ore mineralization is mostly confined to areas of branching and swelling of diabase dikes. In addition, native gold and sulfides, mainly fahlore, pyrite, and chalcopyrite and, locally, Bi sulfosalts also occur in monoquartzites, filling cavities and caverns in porous quartz along with vein minerals.

Two mineral types are distinguished amid ores from the Kairagach deposit. The first, the *gold–quartz* type, is represented by substantially quartz ores with the sulfide (mainly pyrite) content usually being 3–5 wt % or lower. These ores associate spatially with monoquartzite zones and are characterized by massive fabric and, as a rule, low concentrations of useful components, although the Au content can be as high as several hundred grams per ton in some intersections. Quartz is fine-grained to amorphous, with abundant caverns and pores, and contains relicts of enclosing volcanics. Cavities and caverns in such quartz from the Diabazovaya zone are often filled with younger white transparent quartz and barite with fahlores and different sulfide–selenide–telluride mineralization. In this case, the contents of some elements, such as Se, Te, Bi, and Sn, significantly increase. The second, the *gold–sulfide–selenide–telluride type*, is known for the moment only in the Diabazovaya zone. It is represented by vein and lenticular bodies, as well as by stringer–disseminated and nest-shaped quartz, quartz–barite, and barite accumulations with sulfides, sulfosalts, selenides, and tellurides, irregularly distributed both within monoquartzites and within beresite-like rocks in the ore zone. These ores play an important role in reserves of the deposit. They are variable in contents of gold, silver, and other useful components and are characterized by a complex and changeable mineral composition.

By the gold content, ores are subdivided into noneconomic, with the Au content below 3 g/t, and economic ores, which are, in turn, classed as ordinary (up to 10 g/t Au), high-grade (from 10 to 100 g/t Au), and bonanza (above 100 g/t Au) ores. In the Diabazovaya zone, noneconomic ores are usually confined to silicified and beresite-like wall rocks and characterized by the prevalence of Ag over Au and Se over Te (Table 1). The Ag content in ordinary ores is also higher than that of Au, but Te prevails over Se. In high-grade and bonanza ores, gold sharply prevails over Ag and Te over Se. Bonanza and high-grade ores are mostly confined to ore shoots and usually fringed by poorer mineralization. Bonanza ores contain significant quantities of barite, frequently, with aggregates of native gold, fahlores,

Table 2. Main ore minerals and their distribution in ores of the Kairagach deposit

Mineral	Formula	Distribution	Mineral	Formula	Distribution
Native elements			Famatinite	Cu_3SbS_4	++
Bismuth	Bi	++	Chalcostibite	$CuSbS_2$	+
Gold	Au	+++	Enargite	Cu_3AsS_4	+
Copper	Cu	+	Sn(Sb, As) *sulfosalts*		
Tin	Sn	+	Wolfsonite	$Cu_{11}Fe_3Sn_3S_{16}$	++
Silver*	Ag	+	Kesterite	Cu_2ZnSnS_4	+
Tellurium	Te	++	Colusite	$Cu_{26}V_2(As, Sn, Sb)_6S_{32}$	++
Electrum	(Au, Ag)	++	Mowsonite	$Cu_6Fe_2SnS_8$	++
Sulfides			Nekrasovite	$Cu_{26}V_2(Sn, As, Sb)_6S_{32}$	++
Acanthite*	Ag_2S	++	Stannite	Cu_2ZnSnS_4	+
Bornite	Cu_5FeS_4	++	Stannoidite	$Cu_8(Fe, Zn)_3Sn_2S_{12}$	+
Galena	PbS	+++	Stibiocolusite	$Cu_{26}V_2(Sb, Sn, As)_6S_{32}$	+
Covellite	CuS	++	Hemusite	Cu_6SnMoS_8	+
Marcasite	FeS	++	*Tellurides and selenides*		
Pyrite	FeS	++++	Altaite	PbTe	++
Pyrrhotite	$Fe_{1-x}S$	+	Volynckite*	$AgBiTe_2$	+
Sphalerite	ZnS	+++	Hessite	Ag_2Te	++
Chalcocite	Cu_2S	++	Guanajuatite	Bi_2Se_3	+
Chalcopyrite	$CuFeS_2$	++++	Kawazulite	Bi_2Te_2Se	+
Jalpaite*	Ag_3CuS_2	++	Calaverite	$AuTe_2$	+++
Fahlores			Clausthalite	PbSe	+
Goldfieldite	$(Cu,Ag)_{12-x}(Fe,Zn)_x(Te,Sb,As,Bi)_4S_{13}$	+++	Coloradoite	HgTe	+
Tennantite	$(Cu,Ag)_{10}(Fe,Zn)_2(As,Sb)_4S_{13}$	++	Laitakarite	$Bi_4(S, Se)_3$	++
Bi tetrahedrite	$(Cu,Ag)_{10}(Fe,Zn)_2(Sb,As,Bi,Te)_4S_{13}$	+++	Nevskite	Bi(Se, S)	+
Tetrahedrite	$(Cu,Ag)_{10}(Fe,Zn)_2(Sb,As)_4S_{13}$	++++	Petzite	Ag_3AuTe_2	+
Bi(Sb) *sulfosalts*			Rucklidgeite	$PbBi_2Te_4$	+
Aikinite	$PbCuBiS_3$	+++	Sylvanite	$AuAgTe_4$	+
Bismuthite	Bi_2S_3	+++	Cu sylvanite	$Au(Ag, Cu)Te_4$	+
Sb bismuthite	$(Bi, Sb)_2S_3$	+	Sulfotsumoite	$Bi_3Te_2(S, Se)$	+
Hodrushite	$Cu_8Bi_{12}S_{22}$	++	Telluroantimonite	Sb_2Te_3	++
Junoite	$Pb_3Cu_2Bi_8(S, Se)_{16}$	+	Tellurobismuthite	Bi_2Te_3	+
Krupkaite	$PbCuBi_3S_6$	++	Tetradymite	Bi_2Te_2S	++
Lindströmite	$Pb_3Cu_3Bi_7S_{15}$	++	Frohbergite	$FeTe_2$	+
Pecoite	$PbCuBi_{11}(S,Se)_{18}$	++	Stützite	$Ag_{5-x}Te_3$	+
Emplicite	$CuBiS_2$	+++	Phase	AuSbTe	+
Sb emplicite	$Cu(Bi,Sb)S_2$	++	Phase	Au_5SbTe	+
Phase	$(Cu, Ag)(Bi, Pb)_3(S, Se)_5$	+	Phase	$Au_5Sb_2Bi_2Te_{13}$	+
Phase	$(Cu, Ag)(Bi, Pb)_4(S, Se)_6$	+	Phase	$Bi_2(Te, S, Se)_3$	++
Phase	$(Cu, Ag)_2(Bi, Pb)_6(S, Se)_9$	+	Phase	Bi_3Se_2	+
Phase	$(Cu, Ag)_5(Bi, Pb)_9(S, Se)_{16}$	+	*Oxides*		
Phase	$(Cu, Ag)_6(Bi, Pb)_9(S, Se)_{16}$	+	Hematite	Fe_2O_3	++
Sb-(As) *sulfosalts*			Cassiterite	SnO_2	+++
Bournonite	$PbCuSbS_3$	++	Rutile	TiO_2	++
Luzonite	Cu_3AsS_4	++			
Polybasite*	$(Ag, Cu)_{16}(Sb, As)_2S_{11}$	++			
Robinsonite	$Pb_4Sb_6S_{13}$	+			

Note: (++++) widespread, (+++) common, (++) rare, and (+) very rare minerals; (*) minerals registered only in ore body 26 of the Pervaya zone. In compiling the table, data from the following works were used: Badalov and Spiridonov (1983), Badalov *et al*. (1984), Kovalenker (1986), Kovalenker and Heinke (1984), Kovalenker *et al*. (1979, 1984, 1986, 1987), Koneev and Gertman (1997), Spiridonov and Badalov (1983), Spiridonov *et al*. (1983), and original unpublished materials.

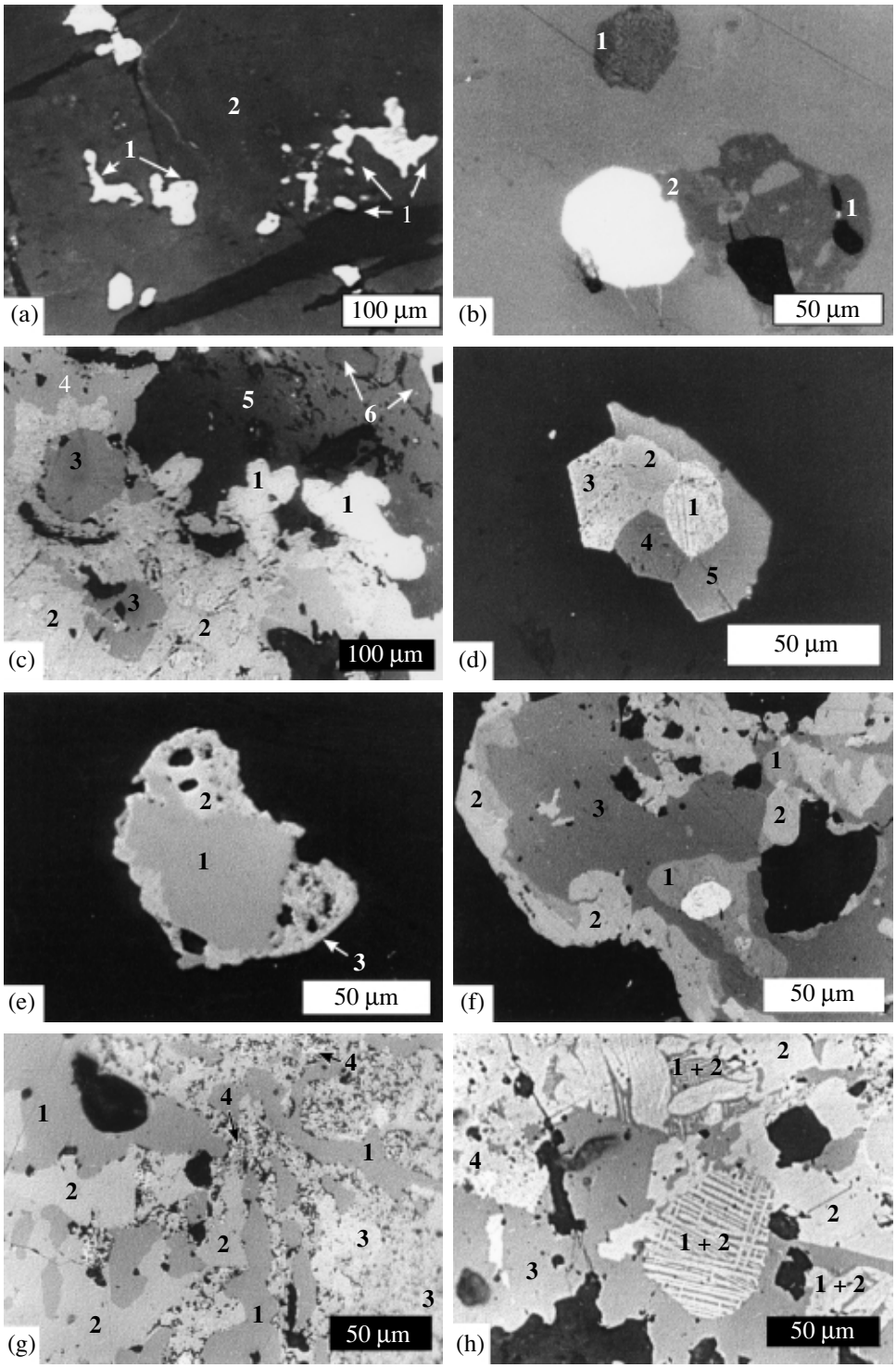

Fig. 5. Ore minerals and their intergrowths in ore of the Kairagach deposit: (a) aggregates of native gold (1) in barite (2), sample 116/86-11, ore body 21; (b) native gold (white), wolfsonite (1), and mowsonite (2) within Se emplicite, sample 147/81-15, ore body 3; (c) aggregates of native bismuth (1) in intergrowth with Se emplicite (2) and nekrasovite (3) within Bi tetrahedrite (4), barite (5), and quartz (6), sample 147/81-5, ore body 3; (d) aggregate of native gold (1), calaverite (2), altaite (3), petzite (4), and chalcopyrite (5) within barite, sample 42/85, ore body 6; (e) frohbergite (1), calaverite (2), and telluroantimony (3) in barite, sample 1031/86-9, ore body 21; (f) native gold of low fineness (white) in stützite (1) within chalcopyrite (2) and tetrahedrite (3) in barite, sample 147/81-7, ore body 3; (g) aggregate of Bi tetrahedrite (1), Se emplicite (2), laitakariite (3), and native bismuth (4), sample 8/83-25, ore body 3; (h) lattice intergrowths of wolfsonite (1) and chalcopyrite (2) within tetrahedrite (3) and emplicite (4) in barite, sample 147/81-20, ore body 3.

tellurides, selenides, sulfobismuthites, and sulfostannates. The integral content of ore minerals in these ores ranges from 3 to 7 wt % and can amount to 15–20 wt % and more in some intersections and separate lumps of ores. Bonanza ores are usually characterized by nest, disseminated, stringer-type, and, locally, brecciated or massive textures.

MINERALOGY OF ORES

The mineral–geochemical composition of commercial ores from the *Diabazovaya zone* is determined by different sulfobismuthites of Cu, Cu and Pb, and Ag and Pb; sulfoantimonites of Cu and Pb; sulfostannates of Cu and Fe; tellurides of Au, Ag, Pb, Hg, Fe and Bi; selenides; sulfoselenides; and Bi sulfoselenotellurides distributed against the background of widespread pyrite, fahlores, and chalcopyrite and rare galena and sphalerite. Ordinary ores are mainly composed of pyrite, chalcopyrite, galena, and sphalerite with thin inclusions of aikinite, hessite, and electrum, as well as subordinate amounts of fahlores. In high-grade and bonanza ores, the general increase in quantities of ore minerals (mainly fahlores), quartz, and barite is accompanied by their enrichment in microinclusions of gold and different sulfosalts, tellurides, and selenides. It should also be noted that tellurium minerals at upper levels are mainly represented by goldfieldite, Te-bearing fahlores where Te occurs in the form of Te^{4+}, and native tellurium (Te^0), whereas, at deeper levels of the ore zone, the proportion of tellurides proper, where Te is represented by Te^{2-}, significantly increases.

At present, over 80 ore minerals have been diagnosed in ores. They are listed in Table 2, which was compiled using original and published data (Badalov and Spiridonov, 1983; Badalov *et al.*, 1984; Kovalenker, 1986; Kovalenker and Heinke, 1984; Kovalenker *et al.*, 1979, 1984, 1986, 1987; Koneev and Gertman, 1997; Spiridonov and Badalov, 1983; Spiridonov *et al.*, 1983). Typical characteristics of minerals and their groups most important for productive associations of gold–sulfide–selenide–telluride ores from the Diabazovaya zone are considered below.

Native Gold

Grains of native gold are of variable morphology: xenomorphic, elongated, lumpy, stringer-shaped, rounded, and oval (Fig. 5a). Sulfides usually enclose single grains of native gold, whereas vein minerals contain their accumulations, frequently confined to contacts between barite and quartz, which are also characterized by elevated amounts of tellurides, selenides and sulfobismuthites.

The remarkable feature of native gold from ores of the Diabazovaya zone is its high fineness (Au/Au + Ag + Cu + Hg), which varies from 992 to 900‰ in more than half of grains, exceeding 800‰ in 85% of them (Fig. 6). Grains of high-fineness native gold are usually confined to either vein minerals (quartz and barite) or pyrite. They also occur often in intergrowths with Au tellurides, altaite, coloradoite, frohbergite, and telluroantimonite (Fig. 5d). Gold of relatively low fineness (<800‰) forms intergrowths with Ag and Ag–Bi tellurides, Bi sulfoselenotellurides, sulfostannates, and fahlores (Fig. 5f). It was established that the native gold fineness increases with depth (Fig. 6). Native gold includes, in addition to silver, notable quantities of Cu (0.2–2.25 wt %) and Hg (0.2–11.26 wt %). The elevated contents of these elements are usually characteristic of gold with relatively low fineness and electrum, confined to ore minerals of productive associations and untypical of native gold of high fineness associated with vein minerals and pyrite. Central parts of grains are frequently composed of low-Hg gold characterized by high fineness, whereas peripheral parts of gold showing low fineness (up to electrum) with a high Hg content. Native gold from the Kairagach deposit is characterized by a stable paragenesis with Sn minerals—sulfostannates (Fig. 5b) and V-bearing (up to 1–2 wt % V) cassiterite, forming close intergrowths with them.

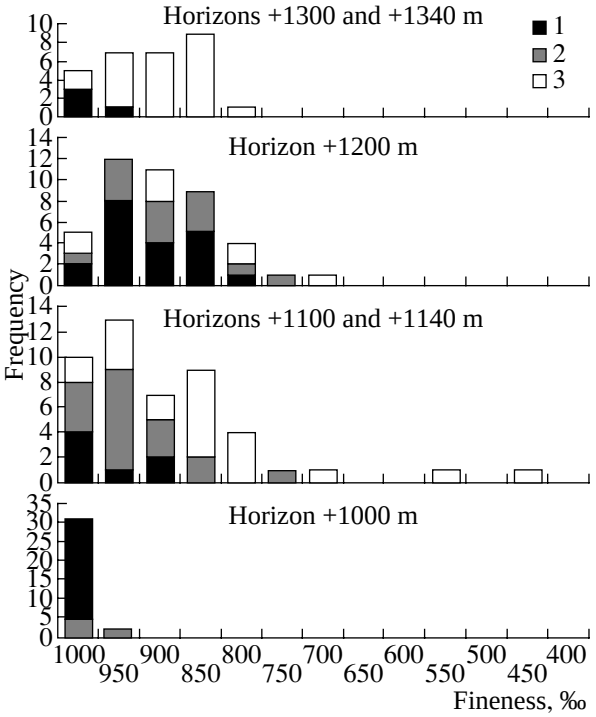

Fig. 6. Histograms of occurrence frequency of different-fineness native gold in ores from the Kairagach deposit (based on the results of electron microprobe analysis): (1) gold in quartz and barite; (2) gold in association with early tellurides and sulfobismuthites; (3) gold in association with hessite, chalcopyrite, and tetrahedrite.

Pyrite

Pyrite is a widespread mineral in the Kairagach deposit. Its age-variable generations, with different mor-

Table 3. Coefficients of paired correlation (*r*) between accessory elements in pyrites of the early productive association from the Kairagach deposit ores

Element	Au	Ag	Ni	Co	Sn	Pb	Bi	Sb	As	Cu
Au		0.72	–0.28	–0.38	0.64	0.43	0.68	0.65	0.64	0.51
Ag			–0.22	–0.26	0.41	0.62	0.38	0.43	0.36	0.55
Ni				0.40	–0.27	–0.19	–0.25	–0.27	–0.28	–0.20
Co					–0.38	–0.18	–0.35	–0.37	–0.25	0.23
Sn						0.31	0.84	0.99	0.94	0.61
Pb							0.33	0.32	0.31	0.48
Bi								0.86	0.80	0.54
Sb									0.95	0.63
As										0.66
Cu										

Note: Significant $r > 0.35$ at $n = 36$ and probability 95%. Strong correlation at $r > 0.7$, stable correlation at $r = 0.5$–0.7, and weak correlation at $r < 0.5$. Negative *r* values indicate an antagonistic relation between elements.

Table 4. Variations in element contents in fahlores of different generations in the Kairagach deposit

Element	Generations of fahlores							
	1 ($n = 5$)		2 ($n = 23$)		3 ($n = 33$)		4 ($n = 48$)	
	a	b	a	b	a	b	a	b
Cu	42.65…40.42	10.28…9.40	44.32…34.27	11.29…9.35	41.55…36.67	10.56…9.50	42.63…30.99	10.96…8.62
Ag	0.78…0.01	0.11…0.00	11.18…0.00	1.80…0.00	0.60…0.00	0.09…0.00	9.53…0.00	1.56…0.00
Fe	5.68…3.16	1.57…0.85	7.11…0.15	2.00…0.04	6.84…1.20	2.04…0.35	5.89…0.04	1.67…0.01
Zn	6.10…2.89	1.39…0.64	4.29…0.03	1.04…0.01	6.28…0.08	1.59…0.02	7.58…0.41	1.90…0.10
Te	1.78…0.00	0.22…0.00	17.16…2.45	2.27…0.30	2.26…0.00	0.28…0.00	4.89…0.00	0.61…0.00
Sb	13.25…0.06	1.68…0.01	22.56…2.94	2.98…0.40	30.58…12.50	4.19…1.62	29.98…10.54	4.17…1.32
As	19.45…9.56	3.87…1.97	12.86…1.71	2.68…0.00	9.95…0.19	2.06…0.04	12.94…0.29	2.64…0.00
Bi	0.45…0.00	0.03…0.00	5.08…0.00	0.40…0.00	9.54…0.55	0.77…0.04	3.34…0.00	0.26…0.00
S	29.31…26.87	13.50…12.92	28.19…22.92	14.17…12.10	26.90…23.42	13.21…12.19	28.17…22.25	14.08…12.00
Se	0.41…0.00	0.08…0.00	1.28…0.03	0.27…0.00	0.59…0.00	0.12…0.00	0.58…0.00	0.12…0.00

Note: *n*, number of determinations; (a) wt %; (b) formula coefficient in calculations for 29 atoms in the formula.

phology of crystalline grains (cubes, cubopentagondodecahedrons, pentagondodecahedrons), are disseminated within wall rock metasomatites and ores or form nests, stringers, and massive aggregates in the latter. Cubes are most common in metasomatites; cubes and cubopentagondodecahedrons in ordinary ores; and cubopentagondodecahedrons, pentagondodecahedrons, and accumulations of rounded grains in high-grade ores. In noncommercial ores, pyrite of earlier generation forms either isolated aggregates or intergrowths with other sulfides (galena, chalcopyrite, and, less commonly, sphalerite), which contain small electrum, aikinite, and hessite inclusions. The pyrite proper sometimes encloses extremely small (several microns) sphalerite, pyrrhotite, magnetite, and rutile grains. In commercial ores, pyrite usually forms close intergrowths with minerals of productive associations—native gold, fahlores, sulfobismuthites, sulfostannates, tellurides, and selenides, with their content and diversity increasing from low-grade to high-grade and bonanza ores. Most of these minerals were formed after pyrite and frequently replace it, cement fractured grains, and fill thin (up to capillary) fissures or form microinclusions.

To define the relations of gold and silver with Ni, Co, Sn, Pb, Bi, Sb, As, and Cu in pyrites of commercial ores from the Diabazovaya zone, paired correlation coefficients (*r*, Table 3) were calculated using data on contents of these elements in 36 bulk samples. It was accepted that $r > 0.7$ corresponds to a strong, $r = 0.7$–0.5 to a stable, and $r = 0.5$–0.3 to a weak correlation. For instance, a strong direct correlation is observed in pyrite between Au and Ag. Gold also shows a stable positive correlation with As, Sb, Bi, Sn, and Cu, a weak positive correlation with Pb, and a negative correlation with Co. In turn, Ag exhibits a strong positive correlation with Pb and Cu and a weak one with Bi, Sn, Sb, and As. There is also a strong correlation between the latter four elements, as well as a stable correlation of them with Cu. This can be explained by close paragenesis of native gold with fahlores, sulfobismuthites, tel-

lurides, selenides, and sulfostannates, whose aggregates occur frequently as microinclusions and/or intergrowths with pyrite. The calculations also show that the integral association Au–Ag–Te–Se–Bi–Sn–Sb–As, which determines the geochemical specialization of ores, is typomorphic for them.

Fahlores

Minerals of this group are second in occurrence after pyrite. They are particularly characteristic of high-grade and bonanza ores developed within ore shoots, where fahlores form relatively large aggregates saturated with inclusions of native gold, Bi sulfosalts, sulfostannates, tellurides, and selenides. This determines the economic significance of fahlores as an accumulator of precious metals, Bi, Te, and Se. Simultaneously, some generations of fahlores themselves are concentrators of Cu, Ag, Bi, Te, and Se, which serve, in case of elevated contents, as mineral-forming elements of these ores.

By chemical composition, fahlores are subdivided into tetrahedrites, goldfieldites, and locally distributed tennantites, although intermediate minerals of the tennantite–tetrahedrite–anivite–goldfieldite row are of main significance. Diagrams in Figs. 7a and 7b show variations in the contents of univalent and bivalent metals and semimetals in fahlores examined.

We defined four different-age generations of fahlores also showing notable differences in chemical composition (Table 4). *The early generation* is mainly represented by tennantites and As varieties of tennantite–tetrahedrite minerals. They are relatively rare and occur in the form of small aggregates in association with pyrite of the early quartz–pyrite stage. *The second generation* is largely developed at upper levels of the deposit, where it is represented by goldfieldite–tennantite–tetrahedrite minerals. The Te contents in these minerals amount to 17 wt %, decreasing with depth to 2–8 wt % (Fig. 7a). Some aggregates show high contents of Ag (up to 11 wt %) and Se (0.2–1.1 wt %). Fahlores of the second generation are characterized by prevalence of univalent metals over bivalent ones relative to stoichiometry and Fe over Zn in bivalent metals (Fig. 7b). As and Sb occur in approximately equal proportions. Fahlores of this generation usually associate with calaverite, altaite, coloradoite, frohbergite, telluroantimony, native Te, and famatinite–luzonite. It is remarkable that a similar association of goldfieldite and high-tellurium fahlore is observed in pipelike bodies of the Kochbulak deposit (Kovalenker *et al.*, 1997), although fahlores of the latter are characterized by lower As contents. Fahlore of the *third generation* shows high (up to 9 wt %, decreasing to 2–5 wt % with depth), elevated (1–3 wt %), and low (<1 wt %) contents of Bi, Te, and Ag, respectively. As and Sb are present in approximately equal proportions, and Fe prevails over Zn (Figs. 7a, 7b). Minerals of this generation closely associate with native gold of high fineness, native Bi, Bi sulfosalts and Bi selenides.

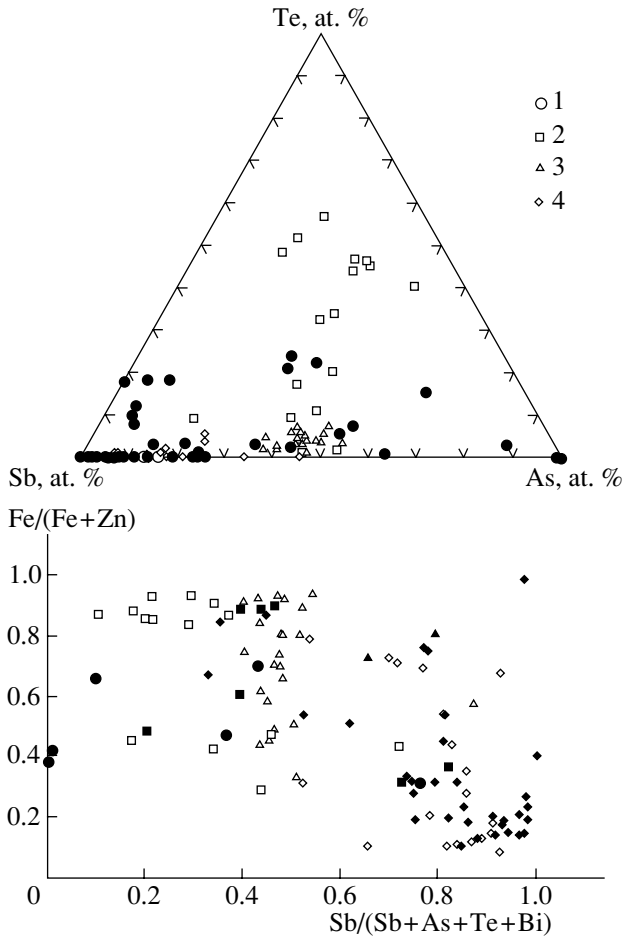

Fig. 7. Composition diagrams for different generations of fahlores of the Diabazovaya zone: (1) early generations; (2) goldfieldite and Te fahlores; (3) Bi fahlores; (4) later generations. Open symbols indicate upper horizons (adits 5, 1, 4), and solid symbols indicate lower horizons (adits 3 + 40, 3, 12).

Fahlores of the second and third generations occur as relict aggregates amid fahlores of the *fourth generation*, which form rather large (up to several millimeters) accumulations and, frequently, intergrowths with chalcopyrite, sulfostannates, chalcostibite, and, sometimes, bournonite. Fahlores of this generation frequently associate with aggregates of native gold with relatively low fineness and Ag tellurides. With respect to composition, the youngest generation of fahlores is characterized by the predominance of the tetrahedrite mineral, prevalence of Zn over Fe, and low (<1 wt %) Ag and Se contents (Fig. 7). Simultaneously, tetrahedrites of the youngest generation, occurring in peripheral parts of ore shoots and associated with bournonite and chalcostibite, are characterized, similarly to the Kochbulak deposit (Kovalenker *et al.*, 1997), by high (up to 10 wt %) Ag contents.

Sulfobismuthites

Bi sulfosalts are characteristic minerals of ores from the Diabazovaya zone. As is seen in Fig. 8, the sulfobis-

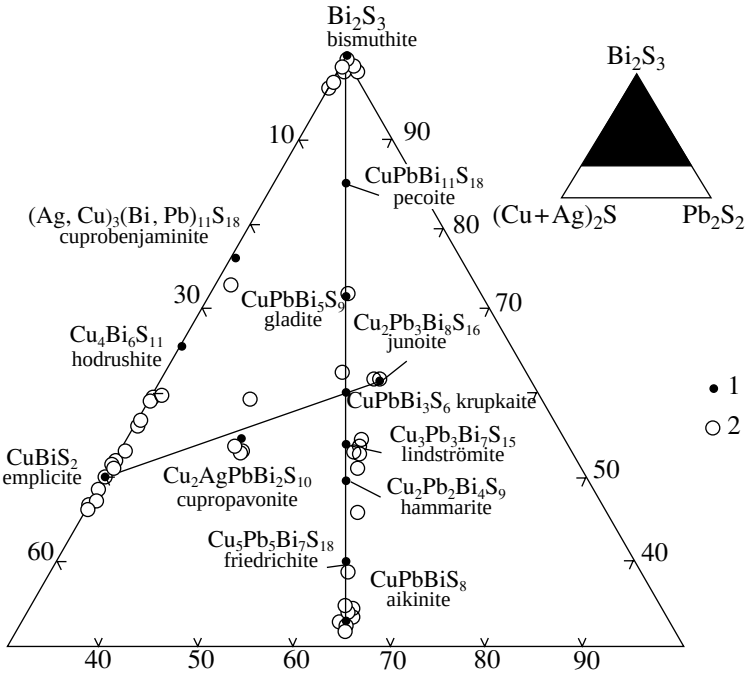

Fig. 8. Composition of By sulfosalts (at. %).

muthites studied are represented by an almost complete set of minerals of the bismuthinite–aikinite (bismuthinite, aikinite, lindströmite, pekoite, krupkaite) and junoite (junoite, emplecite) series, hodrushite, and several rare and poorly studied low-lead natural mineral phases of the Ag–Cu–Pb–Bi–S–Se system (Table 2) that we referred to the pavonite group. These minerals are characterized by high (up to 5–6 wt %) Se and substantial Ag contents, although, in contrast to pavonites, Cu prevails over Ag (Table 5). The minerals mentioned are mainly distributed at upper levels of ore shoots in the Diabazovaya zone, where they compose, along with high-Se bismuthinite, aikinite, emplecite, and hodrushite, productive associations. It should be noted that the Kairagach deposit represents the second locality of hodrushite (Kovalenker *et al.*, 1987), which was first described in Au–Cu–Bi ores of the Banska Hodrusha deposit in Slovakia.

Table 5. Chemical composition (wt %) of unnamed minerals of the Ag–Cu–Pb–Bi–S–Se system

Element	8/83* (7–1)	147/81 (5a)	147/81 (3a)	1031/86 (8b)	1031/86 (8e)	8/83 (9–1)
Ag	3.74	0.83	1.22	3.72	3.80	4.45
Cu	8.48	8.78	14.17	3.85	3.80	4.92
Pb	11.66	10.27	0.51	6.46	6.48	1.93
Bi	55.61	59.71	64.46	64.96	65.15	66.78
S	15.18	15.65	17.83	14.37	13.90	15.69
Se	5.07	4.11	1.89	5.82	6.24	4.49
Te	0.68	–	–	0.37	0.61	0.22
Total	100.42	99.35	100.08	99.54	99.98	98.48
			Calculated formula of minerals			
8/83 (7–1)	$Ag_{1.04}Cu_{4.16}Pb_{1.75}Bi_{7.06}(S_{14.77}Se_{2.00}Te_{0.16})_{15.98}$					
147/81 (5a)	$(Cu_{2.30}Ag_{0.12})_{2.42}Pb_{0.82}Bi_{4.76}(S_{8.13}Se_{0.82})_{9.00}$					
147/81 (3a)	$(Cu_{6.14}Ag_{0.31})_{6.44}(Bi_{8.50}Pb_{0.07})_{8.57}(S_{15.32}Se_{0.66})_{15.98}$					
1031/86 (8b)	$(Cu_{0.69}Ag_{0.39})_{1.08}(Bi_{3.56}Pb_{0.35})_{3.91}(S_{5.13}Se_{0.84}Te_{0.03})_{6.00}$					
1031/86 (8e)	$(Cu_{0.69}Ag_{0.36})_{1.05}(Bi_{3.59}Pb_{0.36})_{3.95}(S_{4.99}Se_{0.91}Te_{0.05})_{5.95}$					
8/83 (9–1)	$(Cu_{0.70}Ag_{0.37})_{1.07}(Bi_{2.89}Pb_{0.08})_{2.97}(S_{4.42}Se_{0.51}Te_{0.02})_{4.95}$					

* Samples (phase number is shown in brackets).
(–) Not detected.

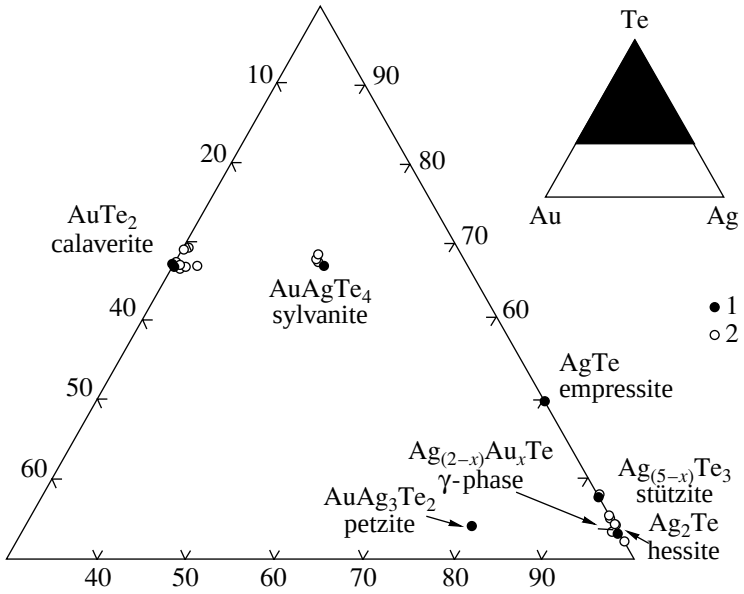

Fig. 9. Composition of minerals of the Au–Ag–Te system (at. %): (1) calculated composition; (2) minerals of the Kairagach deposit.

One of the most characteristic features of Bi sulfosalts developed in high-grade and bonanza ores is their elevated Se content. For instance, according to electron microprobe analysis, the highest Se contents are noted in minerals of the junoite series (up to 4–5 wt %); hodrushite (up to 3.5 wt %); and, as was mentioned above, in natural mineral phases of the Ag–Cu–Pb–Bi–S–Se system. In minerals of the bismuthinite–aikinite series, the Se contents are usually as high as 1–3 wt %, but aikinite distributed in peripheral areas of ore shoots and in transitional zones to ordinary ores is almost barren of Se. In addition to Se, the typical chemistry of the examined sulfobismuthites is determined by a virtually constant admixture of Sb and As, whose contents in some emplicites and bismuthinites can be significant. The significance of Sb as a typomorphic element of ores from the Kairagach deposit is emphasized by the occurrence of sulfosalts of mixed Sb–Bi composition. According to our observations, ores developed at the level of adit 12 contain antimonian bismuthinites (2–8 wt % Sb) and sulfosalt with intermediate composition (Bi = 66.50, 66.17; Sb = 14.07, 11.55; S = 19.94, 16.42; Se = 0.00, 7.40) between bismuthinite (Bi_2S_3) and horobetsuite (~$BiSbS_3$). Sb–Bi sulfosalts also include a mineral discovered for the first time, which contains (wt %) Cu 22.67, Bi 26.78, Sb 25.27, S 22.36, and Se 0.79. Its idealized formula can be presented as $[Cu_5Sb_3Bi_2(S,Se)_{10}]$ or, if it is assumed that this mineral is Bi chalcostibite, as $[Cu(Sb_{0.6}Bi_{0.4})(S,Se)_2]$. Bi-free chalcostibite was also found in ores at the level of adit 3 in association with the youngest fahlore and bournonite.

Tellurides and Selenides

Te and Se minerals are widespread in ores of the deposit. Our and other (Badalov *et al.*, 1984; Spiridonov and Badalov, 1983) investigations revealed a large group of binary, triple, and more complex compounds, including rare and, probably, new ones (Table 2), which can be classed with the Au–Ag–Te, Ag–Pb–Bi–Sb–Te, and Bi–Te–S–Se systems. Tellurides form mostly small (30–300 μm) isolated inclusions or aggregates in barite, at contacts between the latter and quartz, amid fahlore accumulations (less commonly), and in quartz (at deeper levels).

The examined minerals of the Au–Ag–Te *system* include native gold, tellurium, calaverite, sylvanite, petzite, hessite, and stützite, which enclose almost all the gold and most of the silver of the deposit. These minerals occur either in the form of isolated inclusions or close intergrowths with each other (Figs. 5a, 5d, 5f) among vein and ore minerals. Peculiarities in the true composition and paragenetic relationships between minerals of this system are demonstrated by the triple diagram in Fig. 9. At deeper levels, calaverite associates also with frohbergite and telluroantimony (Fig. 5e).

According to our data, *calaverite* is characterized by stoichiometric relationships between the main components. At upper levels, it contains insignificant (up to 0.3–0.4 wt %) quantities of silver, which increase locally up to 1.7–1.8 wt % at lower levels. The mineral encloses almost ubiquitously small quantities of Se (up to 0.34 wt %) and, at lower levels, Cu (up to 0.5–0.9 wt %) and Sb (up to 1.6–3.0 wt %). It is remarkable that, precisely at lower levels, minerals of gold-productive associations include, along with calaverite, several phases of Au–Sb–Te composition with a variable number of elements. According to electron microprobe analysis, one such phase contains 79.47, 0.17, 10.61, and 9.05 wt % of Au, Ag, Te, and Sb, respectively, which corresponds to the idealized formula Au_5SbTe.

The other phase contains the same elements, but in other proportions (wt %): Au 44.37, Te 26.38, Sb 28.04, and Se 0.41. This composition corresponds well to the idealized formula AuSbTe. A third discovered natural phase includes Bi as well, in addition to Au, Sb, and Te (wt %): Au 31.58, Sb 8.87, Bi 5.81, and Te 54.23. The calculated formula of this phase is close to the stoichiometry of $Au_5Sb_2Bi_2Te_{13}$, and the phase belongs probably to the nagyagite–buckhornite group. Calaverite associates primarily with native gold of high fineness and petzite at upper levels and mainly with telluroantimony, frohbergite, and, sometimes, native tellurium and sylvanite at lower levels.

Sylvanite, which occurs mainly at relatively deep levels of the deposit and is noticeably subordinate to calaverite, usually contains, in addition to stoichiometric Au, Ag, and Te, a substantial (up to 0.4 wt %) admixture of Cu. According to electron microprobe analysis, one small sylvanite aggregate in barite from adit 12 corresponds in composition (wt %: Au 24.27, Ag 7.31, Cu 3.15, Te 63.26) to the idealized formula $[Au(Ag_{0.6}Cu_{0.4})Te_4]$; i.e., it is transitional within the sylvanite ($AuAgTe_4$)–kostovite ($AuCuTe_4$) isomorphic row. Noteworthy is the fact that kostovite and similar phases intermediate between sylvanite and kostovite are characteristic also of high-grade Au–Te ores in tubular bodies of the Kochbulak deposit (Kovalenker *et al.*, 1997).

By time of formation, youngest among tellurides of the Kairagach deposit are *hessite, stützite, tetradymite, volynskite*, and *rucklidgeite*, which associate with gold of low fineness (Fig. 5f) and Bi sulfoselenotellurides and selenides. The latter compounds include relatively rare minerals such as *guanajuatite* (Bi_2Se_3), *kawazulite* (Bi_2Te_2Se), *laitakariite* [$Bi_4(Se,S)_3$] (Fig. 5g), *nevskite* [Bi(Se,S)], *selenosulfotsumoite* [$Bi_3Te_2(S,Se)$], and still unnamed natural phases [$Bi_2(Te,Se,S)_3$] and [$Bi_3(Se,S)_2$]. All these minerals are characteristic of gold-productive associations and occur only within ore shoots, mainly at their upper levels. The association in question also includes native tellurium with rather high (3.40–10.25 wt %) Se content. Small isolated aggregates of this mineral are usually confined to barite. Although selenides are rare at deeper levels, where only Bi selenotelluride (kawazulite) is established, some Sb–Bi sulfosalts contain significant (from 2.89 to 10.14 wt %) quantities of Se as well. An elevated Se content is also characteristic of sulfotsumoite (wt %: Bi 68.89, Sb 0.69, Te 24.06, S 3.27, Se 3.09), first established in ores of the Kairagach deposit.

Sulfostannates

Sulfostannates represent one of the typomorphic mineral groups in high-grade and bonanza ores (Table 2). They include mowsonite, stannoidite, stannite, kesterite, nekrasovite, wolfsonite, hemusite, and several still unnamed Cu–Sn sulfosalts with variable proportions of elements. We include into this group also Sn-bearing colusite and stibiocolusite, connected by transitions with isostructural nekrasovite. Sulfostannates never form large accumulations in ores and are usually represented by small (up to 50–100 μm), although abundant, rounded or xenomorphic aggregates confined most commonly to fahlore or barite and quartz. These minerals usually occur in close intergrowths with each other, as well as with pyrite (sometimes in the form of lattice intergrowths; Fig. 5h), native gold, selenian emplectite (Fig. 5b), native bismuth, and other sulfoselenides and sulfobismuthites (Fig. 5c). Sulfostannate aggregates frequently contain accumulations and separate grains of V-bearing (up to 1–2 wt %) cassiterite and native tin (Badalov *et al.*, 1984). Inasmuch as chemical composition and parageneses of sulfostannates in ores of the Kairagach deposit are considered in detail in several works (Kovalenker and Heinke, 1984; Kovalenker *et al.*, 1984, 1986; Spiridonov *et al.*, 1983), we note only that they contain, similarly to other ore minerals from this deposit, Sb, As, and Se admixtures.

PARAGENETIC RELATIONSHIPS AND MINERAL FORMATION SUCCESSION IN ORES

As is seen from the study of structural–textural ore properties, ore mineralization and wall rock hydrothermal alterations occurred in a certain succession, which corresponds to stages of the mineral-forming processes in the Kochbulak deposit (Kovalenker *et al.*, 1997). We defined four main stages of mineral formation: pre-ore metasomatic, early productive, main productive, and post-productive.

The stage of pre-ore metasomatites, which preceded the productive stage, included formation of quartz metasomatites of the secondary quartzite type, pyrophyllite–diaspore–kaolinite–alunite rocks of the advanced argillization type, and quartz–carbonate–sericite alterations of the beresite type. The main role in composition of mineralization of the *early productive, or gold–pyrite–quartz stage* belongs to minerals of the gold–pyrite–quartz association. It is represented by disseminated sulfides (mainly pyrite, less commonly chalcopyrite, and rarely sphalerite and galena with very finely dispersed inclusions of native gold) in vein and gray metasomatic quartz developed after andesite–porphyries.

Minerals of the *main productive, or gold–fahlore–sulfosalt–telluride stage* determine the mineralogical–geochemical properties of the deposit and its gold-ore potential. They formed either immediately after the productive gold–pyrite–quartz stage or after formation of the interproductive (according to N.V. Petrovskaya) association of gangue minerals. The main productive stage combines several mineral associations, usually similar in formation time and frequently closely spaced. The earliest of them is the gold–quartz–barite association, which is represented by accumulations of native high-fineness gold in quartz–barite aggregates and characterized by almost synchronous deposition of gold, quartz, and barite. Deposition of these minerals could be caused by the removal of H_2S from the hydro-

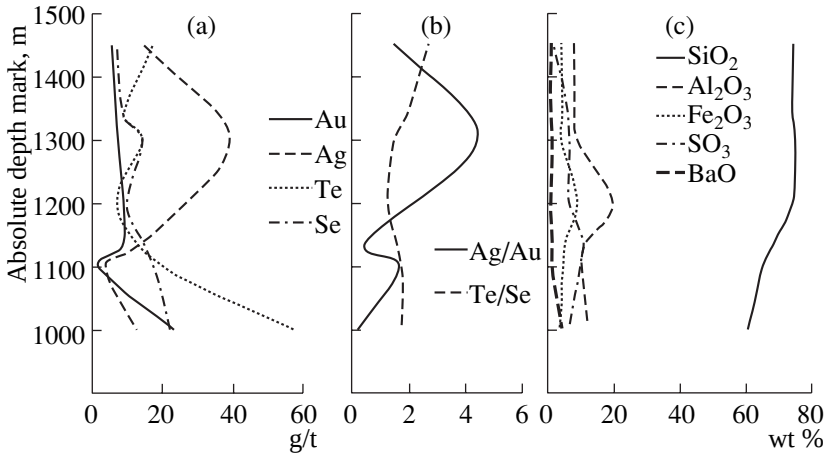

Fig. 10. Distribution of Au, Ag, Te, and Se contents (a) and ratios (b) and contents of petrogenic elements (c) in ores through the vertical cross section of the Diabazovaya zone.

thermal solution due to its boiling at or near the water table. Such a process was suggested to explain formation of gold–quartz–barite bonanza ores in the Summitville deposit in Colorado, the United States (Cunningham, 1985).

At upper levels of the Diabazovaya zone, gold–quartz–barite mineralization is superimposed on metasomatic quartz, which usually hosts the most significant accumulations of finest native gold. The occurrence of chalcedony-like quartz is an indicator of a sharp oversaturation of the ore-forming solution with silica (Fournier, 1985). At deeper levels, quartz is better crystallized and gold aggregates fill interstices between its grains.

The stage under consideration also includes the goldfieldite–famatinite association, which is mainly developed at upper levels of the Diabazovaya zone, where it is represented by small (up to several micrometers) aggregates of these minerals in barite and quartz or relicts in fahlores of younger generations. Goldfieldite is subjected, similarly to the Kochbulak deposit (Kovalenker *et al.*, 1997), to hypogenic decomposition with formation of chalcopyrite, tetrahedrite, and tellurides, which indicate the change of the oxidizing environment for a more reducing one.

The association of native gold with early tellurides, represented mainly by altaites and less common calaverite, frohbergite, coloradoite, telluroantimony, and others, is widespread in barite-enriched ore shoots (Figs. 5d, 5e). It occurs almost throughout the entire ore zone except for its near-surface level. In its formation time, the sulfobismuthite–sulfostannate–gold association is similar to the closely situated association of early tellurides, although it is not inconceivable that sulfobismuthites localized at deeper levels formed slightly earlier than tellurides. This association, probably, also includes relatively large aggregates of native bismuth confined to barite and sulfide accumulations (Fig. 5c).

The relatively later bismuth–sulfoselenide association is represented by native bismuth, laitakariite, and other sulfoselenides, as well as chalcopyrite (Fig. 5g), which replaced selenian sulfobismuthites after their hypogenic decomposition under changed physicochemical environments. The earliest among sulfobismuthites are minerals of the bismuthite–aikinite and junoite series that associate with Bi-enriched fahlores. They are spatially close to the gold–telluride association, although seem to have formed slightly later, which is evident from overgrowing of early Se-enriched telluride aggregates by native tellurium. The latter is, in turn, sometimes overgrown by chalcopyrite. The association of hessite, low-fineness gold, and chalcopyrite (Fig. 5f) is one of the latest mineral associations formed at the main productive stage.

Mineralization of the *post-productive, or quartz–carbonate–barite stage* is represented by thin veins and stringers that cut products of all earlier stages. These veins and stringers sometimes contain, in addition to quartz, carbonates, and barite, variable quantities of sulfides, mainly galena and sphalerite, accompanied by less common chalcopyrite, pyrite, marcasite, and tetrahedrite.

MINERALOGICAL–GEOCHEMICAL ZONING

Spatial changes in the chemical composition of ores in the Diabazovaya zone were defined using data on petrogenic and ore-forming elements, including precious and rare metals, in group and trench bulk samples that characterize ore mineralization from the surface (~+1400 to +1450 m) up to the level of adit 12 (+1000 m). These works were carried out by specialists from the Tashkentgeologiya enterprise in the course of deposit exploration. The results of the data processing are demonstrated by the vertical section (Figs. 4b, 4c) and the diagrams in Fig. 10. The Diabazovaya ore zone shows the successive change of low-grade for high-grade ores downward and in the southeastern direction. Three longitudinal zones are distinguished there: with low-grade Au–Ag ores (Au/Ag = 0.1–1.0), high-grade

Table 6. Average contents of accessory elements (g/t) in pyrite concentrates

Horizon	Au	Ag	Se	Te	Ag/Au	Te/Se	Ni	Co	Sn	Pb	Zn	Bi	Sb	As	Cu
Surface (n = 18)	14.5	33.9	149.4	500.0	2.33	3.35	49	90	10	575	89	9	106	883	893
Adit 1 (n = 44)*	17.6	22.0	241.2	554.5	1.25	2.30	62	154	13	380	2500	45	65	65	2851
Adit 3 (n = 33)	56.1	31.4	166.4	600.0	0.56	3.60	86	49	5	3709	346	96	237	1718	1510
Adit 12 (n = 22)	192.2	88.5	71.6	360.8	0.46	5.04	91	62	6	1927	346	75	170	914	1366
Total (n = 107)	66.5	42.6	190.4	568.5	0.64	2.99	79	106	10	1793	1221	65	153	893	2069

* Quantitative chemical and spectral analysis was performed at IGEM (analysts: G.E. Belousov and V.A. Sychkova). Other determinations were performed at the Central Chemical Laboratory of the State Geological Enterprise Tashkentgeologiya by assay spectral (Au, Ag), atomic absorption (Se, Te), and spectral (other elements) methods.

mixed Ag–Au and Au–Ag ores (Au/Ag from 0.1 to 1.0 and more), and high-grade substantially gold ores (Au/Ag = 1.0–10.0).

The SiO_2 content decreases from the surface downward to the level of adit 12 (from 74.5 to 60.4%), whereas the SO_3 content increases in the same direction (from 1.62 to 9.86%) against the background of strongly variable BaO content and its relatively high values at deeper horizons (Fig. 10c). Maximum Au contents (and very low Ag concentrations) are characteristic of ores at deeper levels near the Ogranichivayushchii fault. In this area, native gold occurs, more frequently than in others, in association with fahlore and chalcopyrite confined to quartz–barite aggregates. Gold distribution through the vertical section of the ore zone is characterized by wavy patterns: its content first grows, reaching maximum values at the level of adit 3 + 40, to then decrease again downward (Fig. 10). Simultaneously, maximum Ag contents are registered at the level of adit 1, whereas the Ag/Au ratio decreases monotonously with depth (from >1 to 0.1; Fig. 10b), which indicates transition from Au–Ag ores at upper levels to substantially gold ores at lower levels.

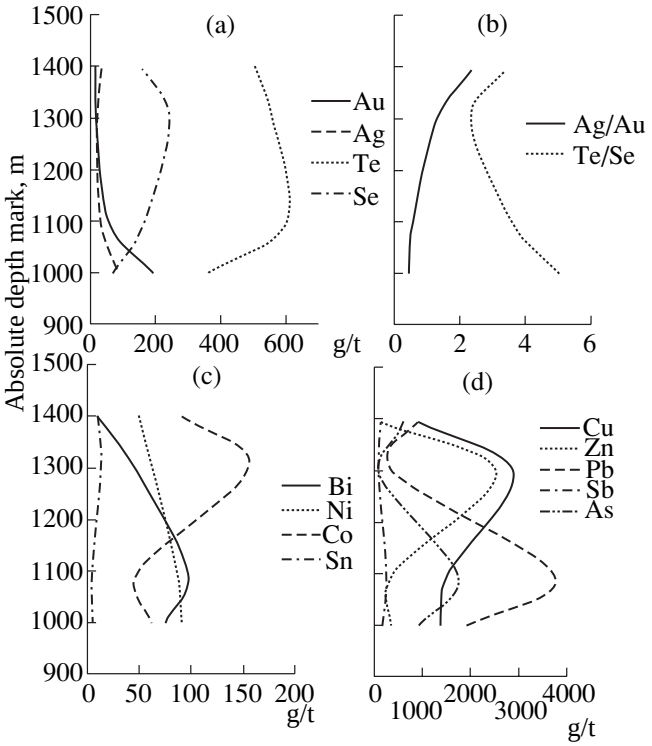

Fig. 11. Distribution of Au, Ag, Te, and Se contents (a) and ratios (b) and other accessory elements in pyrite through the vertical cross section of the Diabazovaya zone.

The zone of mixed ores is usually characterized by high Ag, Te, Se, and Bi contents. As a rule, these elements occur together, although, at deeper levels, there are separate areas enriched either in Te, Se, or Ag (Fig. 10). At upper levels of ore bodies (adit 5), Te and Se occur as rare telluride and selenide inclusions in later fahlores. They formed, probably, as a result of goldfieldite decomposition. At a slightly lower level (adit 1), Te and Se are present both as constituents of goldfieldite and in the form of abundant small inclusions of tellurides, native tellurium, selenides, and their aggregates within barite. In general, upper levels are characterized by the prevalence of Se over Te, because tellurides are of limited development there, whereas significant amounts of Se are contained in sulfobismuthite and also in selenides and sulfoselenides. At deeper levels (adits 4 and 3) closer to the ore-controlling fault, the Te content, which is mostly present in telluride and native forms, increases and prevails over Se. It is notable that curves of the changes in Te and Se contents are similar to those of BaO (Fig. 10), because minerals concentrating these elements are usually confined to barite aggregates. Simultaneously, the Cu contents throughout the vertical section of ore bodies remain almost the same, because the distribution of chalcopyrite and fahlores is relatively uniform. On the contrary, the Bi contents decrease from the upper to the lower levels by several times (from approximately 0.1 to 0.02 wt %) and, beginning from the level of adit 1, correlate with the Pb contents, because most Pb is enclosed here in sulfobismuthites.

A similar distribution pattern of contents of Au, Ag, and other ore elements is revealed in pyrite concentrates (~95 wt % pyrite) that characterize ores from different depth levels of the Diabazovaya zone, from the surface to the level of adit 12 (Table 6; Fig. 11). The Au

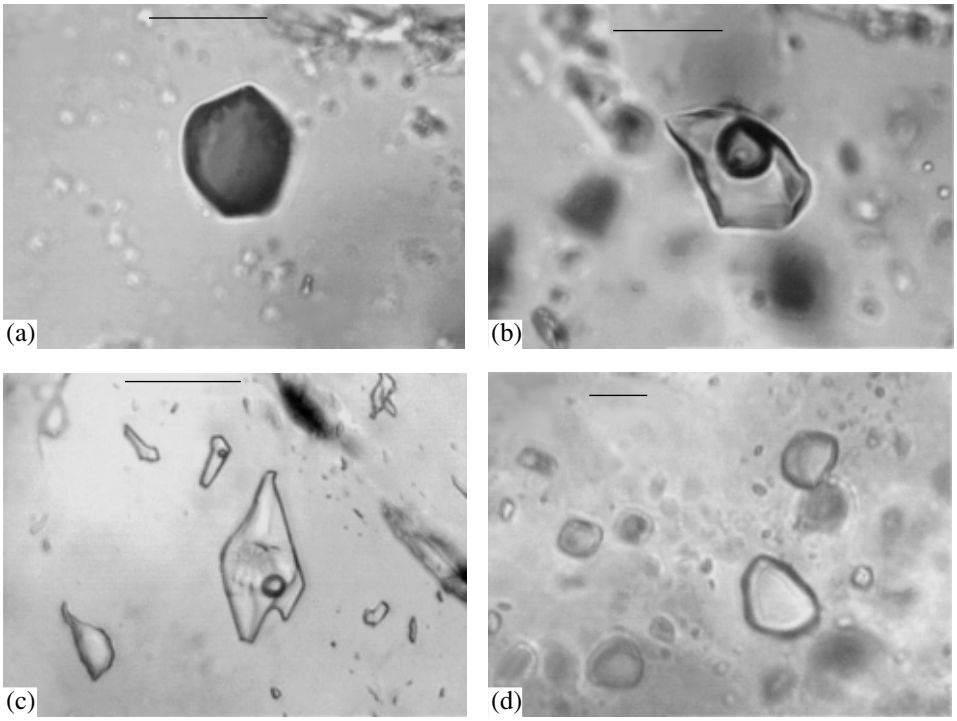

Fig. 12. Primary fluid inclusions in quartz and barite from productive mineral associations of ores in the Kairagach deposit: (a) vapor-rich in quartz, sample 128/83; (b) two-phase in quartz (T_{hom} = 309°C), sample 128/83; (c) two-phase in quartz (T_{hom} = 158°C), sample 64/82; (d) single-phase, liquid, low-temperature in barite, sample 42/85. The bar length is 10 μm.

contents decrease gradually up to the level of adit 3 (+1100 m) and then increase sharply. The Ag contents first slightly decrease up to the level of adit 1 (+1350 m) and then gradually grow (Fig. 11a). The Ag/Au ratio decreases with depth, indicating that the intensity of accumulation of gold at deeper levels is significantly higher than of Ag (Fig. 11b). At the level of adit 1 and in the northeastern flanks of adits 4 and 3 + 40, i.e., in immediate proximity to the Ogranichivayushchii fault, mainly the early association of native gold of high fineness in the quartz–barite aggregate (Fig. 5a) is developed. At the same time, gold from the level of adit 3 near the Karatash ore-controlling fault is of later generation and occurs only in the form of inclusions in fahlores. The Se and Te contents in pyrite concentrates first increase with depth and then diminish (Fig. 11a). Nevertheless, maximum Se contents are registered at the level of adit 1, whereas maximum Te contents occur substantially deeper, at +1100 to +1200 m. Variations in the Te/Se ratio suggest that the highest Te contents are peculiar to pyrite concentrates that characterize the upper and lower levels of the deposit, while the maximum Se content corresponds to the upper to middle part of the ore zone (Fig. 11b), although Te always prevails over Se. The Sb and As contents vary synchronously with the wavy patterns, showing minimum and maximum values at the levels of adits 1 and 3, respectively (Fig. 11d). The opposite distribution trend is characteristic of Co, whereas Ni contents show a gradual increase with depth (Fig. 11c).

RESULTS OF FLUID INCLUSION STUDY

Methods

Microthermometric investigations were performed using a THMSG-600 heating and freezing stage (Linkam). Application of a high-resolution objective (Olympus) with a magnification of 80 made it possible to observe fluid inclusions 10 μm across and larger. Temperatures of phase transitions were measured in the interval from –196 to +600°C, with an accuracy of ±0.2°C in the interval from +20 to –20°C and at least ±1.0°C beyond these limits. The pressure was determined only for a heterogeneous fluid, using syngenetic vapor-rich and vapor-liquid inclusions, as a sum of the pressure of saturated water vapor and of carbon dioxide (if it was registered during inclusion cooling).

The salt content was estimated based on the temperature of ice melting calculated for the H_2O–NaCl system and using data from (Bodnar and Vityk, 1994). The density of NaCl water solution was calculated using the program FLINCOR version 1.21 (Brown, 1989). It should be noted that, in the course of cryometric studies, single-phase inclusions sometimes showed metastable ice melting under positive temperatures, which suggests negative intravacuole pressure. Therefore, salt concentrations that were calculated using ice-melting temperatures for single-phase inclusions can be underestimated by several percent (Roedder, 1984).

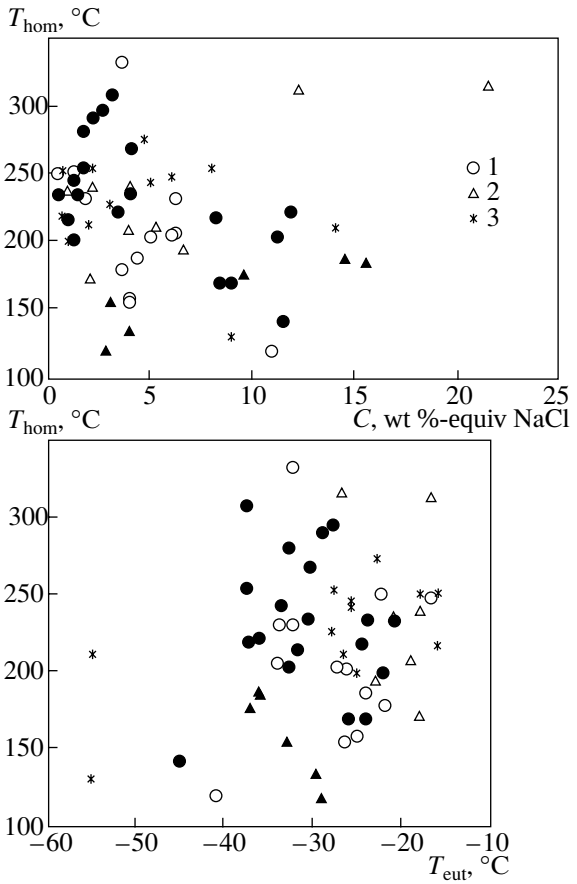

Fig. 13. Variations in main parameters for primary and primary–secondary fluid inclusions in quartz (1) and barite (2) from the Diabazovaya zone and in quartz from the Pervaya zone (3). Open and solid symbols indicate upper and lower horizons, respectively.

Types of Fluid Inclusions

The study, in transmitted light, of bilaterally polished plates 0.3–0.5 mm thick prepared from quartz and barite samples that were taken in the Diabazovaya and Pervaya ore zones revealed rare fluid inclusions 0.5–35 μm across and shaped as negative crystals or having an irregular form. Uniform distribution of inclusions throughout the host mineral and their local confinement to growth zones served as criteria for their primary character. Fluid inclusions confined to fissures limited by outer zones of the crystal growth were referred to the primary–secondary type, which includes most of the examined inclusions. Fluid inclusions tending to fissures crossing boundaries between grains of vein minerals were considered as secondary inclusions (Roedder, 1984).

Quartz and, less commonly, barite characterizing the examined hydrothermal mineralization was established to contain single-phase, vapor-rich (Fig. 12a) and syngenetic two-phase, liquid–vapor fluid inclusions (Figs. 12b, 12c), in which vapor vacuoles compose from 5 to 30 vol %. The co-occurrence of such fluid inclusions is usually considered as an indicator of hydrothermal fluid boiling (Roedder, 1984). They represent mainly the primary and primary–secondary types of fluid inclusions. Simultaneously, secondary fluid inclusions, occurring mostly within barite, are represented by single-phase inclusions filled with water solution (Fig. 12d), which points to their entrapment under a temperature of <50°C (Roedder, 1984). It should be also noted that freezing of a vapor-rich fluid inclusion results in formation of a small carbon dioxide crystal that turns into vapor under heating in the temperature interval of –74 to –68°C, indicating the low density of CO_2. One fluid inclusion (sample 65/82) showed carbon dioxide melting under a temperature of –56.6°C, with its subsequent homogenization into vapor at –50°C.

Results of Thermometric Investigations

About 100 samples characterizing bonanza, high-grade, and ordinary ores from the Diabazovaya and Pervaya zones were collected to study fluid inclusions by the microthermometric method. The study of plates prepared from these samples revealed, however, that fluid inclusions suitable for quantitative thermo- and cryometric studies occurred in only 23 of them. Table 7 demonstrates the results of the study of 446 individual inclusions in quartz and barite characterizing hydrothermal mineralization of the Diabazovaya and Pervaya zones. We referred a significant share of the examined fluid inclusions (147) to the secondary type and excluded them from further analysis, since they have no direct relation to the ore-forming process proper. Therefore, the diagrams in Fig. 13 demonstrate only the data on primary and primary–secondary fluid inclusions, arranged according to their confinement to the upper and lower levels of deposits (accordingly, above and below adit 4).

The data obtained (Table 7; Fig. 13) show that mineral-forming fluids are characterized by wide variations in physicochemical parameters: homogenization temperature (T_{hom} – 333… <50°C), pressure (P = 120–20 bar), eutectic temperatures (T_{eut} = –55 to –12°C), salt concentration (C = –21.5–0.4 wt % NaCl equiv.), and solution density (d = 1.11–0.67 g/cm^3). With elimination of secondary fluid inclusions from the analysis, these intervals were substantially narrowed. For instance, the highest T_{hom} (>330°C) and pressure (120 bar) values are obtained for primary fluid inclusions in the early gold-free coarse-grained white quartz from the 2nd Parallel zone, located beyond the distribution contour of economic ores. In primary and primary–secondary fluid inclusions discovered in quartz from mineralization of the early gold–pyrite–quartz stage, T_{hom} varies from 309 to 201°C, averaging 260°C at n = 114. Lower T_{hom} values (249–119°C, averaging 190°C at n = 66) are registered for fluid inclusions from quartz and barite belonging to mineral associations of the main productive gold–fahlore–sulfosalt–telluride stage. Approxi-

Table 7. Results of microthermometric studies of fluid inclusions in minerals from ores of the Kairagach deposit

Sample number	Mineral	*n* (fluid inclusion type)	T_{hom}, °C	T_{eut}, °C	$T_{melt\ NaCl}$, °C	*C* of salts, wt %-equiv NaCl	*d* of fluid, g/cm^3	*P*, bar	Adit	Sample characteristic
					Diabazovaya zone					
2/86	Q	3 (p)	252	–23…–22	–0.7…–0.2	1.2…4.0	0.79…0.80	–	5	Quartzite with stringers of sulfides (Bl + Cp + Bi-ss)
		1 (p–s)	249	–17	–9.5	13.4	0.92	–		
10/86		7 (p–s)	318…315	–27…17	–18.6…–8.4	21.4…12.2	0.83…0.92	–		Q–Ba stringer with Gn
64/82	Q*	7 (p)	333	–32.5	–2.1	3.5	0.67	120	1	Early white crystalline Q from the second vein (parallel) zone
	Q	29 (p–s)	234…231	–34…–32	–3.8…–1.1	6.2…1.9	0.91…1.02	–		
		7 (p–s)	203–158	–26…–25	–2.4…–2.2	4.0…3.7	0.90…0.94	–		
		34 (s)	120	–41.0	–7.3…–7.2	10.9…10.7	0.84	–		
65/82	Q*	6 (p–s)	205…155	–27…–26	–3.5…–2.8	5.7…4.7	0.91…0.95	27…12		Bonanza Q + Bar + Fo + Bi-ss + Au + Sn-ss + Cp mineralization in quartzite
	Q	8 (s)	107…<50	–54…–53	–18.8…–11.2	21.5…15.2	1.11…1.10	–		
	Ba	13 (s)	<50	–25…–23	–2.2…–1.4	3.7…2.4	1.01…1.00	–		
8/83		4 (p)	241	–18…–12	–2.4…–1.3	4.0…2.2	0.83…0.85	–		
		3 (p–s)	211…209	–19	–3.2…–2.3	5.3…3.9	0.89…0.90	–		
		6 (p–s)	195…173	–23…–18	–4.1…–1.2	6.6…2.1	0.89…0.94	–		
64a/84	Q	8 (p–s)	187…179	–24…–22	–2.6…–2.1	4.3…3.6	0.91…0.92	–	4	Q breccia with Fo, tellurides, and Au
42/85	Ba	6 (p)	237	–21	–0.5	0.9	0.83	–		Q–Ba vein with Au, Bi-ss, and Tdm
		41 (s)	104…<50	–36…33	–5.3…–5.2	9.7…6.3	1.0…1.03			
103/89		17 (p–s)	134…119	–30…–29	–2.4…–1.7	4.0…2.9	0.96…0.97	–	3 + 40	Au–Q–Ba association
104/89		22 (s)	115…<50	–53…–50	–7.1…–6.5	10.6…9.9	0.81…0.85	–		
68/86	Ba	3 (p–s)	170	–26…–24	–5.8…–5.4	9.0…8.4	0.96	–	3	Stringers of ore Ba in silicified porphyrite
		12 (s)	<50	–53…–50	–12.2…–6.2	16.2…9.5	1.10…1.05	–		
108/89	Q	10 (p)	292…235	–29…–31	–1.3…–2.4	4.9…2.2	0.86…0.74	–		Amethyst-like Q
		11 (p–s)	142	–45	–7.8	11.5	1.01	–		

Table 7. (Contd.)

Sample number	Mineral	*n* (fluid inclusion type)	T_{hom}, °C	T_{eut}, °C	$T_{melt\ NaCl}$, °C	*C* of salts, wt %-equiv NaCl	*d* of fluid, g/cm^3	*P*, bar	Adit	Sample characteristic
Kai-21	Ba	17 (s)	188…<50	–37…–36	–10.5…–8.5	14.5…12.3	0.99…1.08	–	12 + 25	Aggregate of pink–gray Ba + An
128/83	Q*	19 (p)	309…281	–38…–33	–1.8…–1.0	3.1…1.7	0.70…0.76	90…65	12	Au productive association
		66 (p–s)	254…244	–38…–32	–2.0…–0.7	3.4…1.2	0.80…0.87	–		
G232-9		3 (p–s)	219	–25…–24	–5.3…–5.2	8.3…8.1	0.91	–		Q–Ba aggregate
Kai-32		9 (p–s)	234	–21	–0.3	0.5	0.82	–		Q–Ba aggregate with Py, Fo, and Cp
Kai-33	Ba	6 (p–s)	186…177	–37…–36	–11.5…–6.3	15.5…9.6	0.95…1.01	–		Q–Ba aggregate with Fo, Fm, Bour, and Au
Kai-34	Q	5 (p–s)	234…201	–24…–22	–0.8…–0.7	1.4…1.2	0.83…0.88	–		Crystals of smoky Q in An
		8 (p–s)	223…204	–36…–33	–8.1…–7.6	11.8…11.2	0.94…0.95	–		
Kai-43		2 (p)	297	–28	–1.5	2.6	0.72	–		Q–Ba aggregate with Py, Fo, Cp, Au, and tellurides
	Ba	3 (p–s)	155	–33	–1.8	3.1	0.94	–		
					Pervaya zone					
136/87	Q*	7 (p)	227…212	–28…–27	–1.6…–1.1	2.7…1.9	0.85…0.87	25…20	9	Q–Car vein with Py, Cp, Fo, and Ag–As–Sb sulfosalts
141/87	Q	8 (p)	275…252	–23…–18	–2.8…–0.4	4.7…0.7	0.76…0.82	–		
146/87		9 (p–s)	254…247	–28…–27	–5.2…–3.2	8.1…5.7	0.87…0.86	–		Gray Q with Car, sulfides, and Ag sulfosalts
		8 (p–s)	211…130	–55	–10.6…–6.0	14.6…9.2	0.97…1.00	–		
143/87	Q	11 (p)	243…200	–26…–25	–3.0…–0.5	5.0…0.9	0.85…0.87	–		Gray Q
542/87		7 (p)	253…218	–16	–1.3…–0.4	2.2…0.7	0.81…0.85	–		Q with Cp, Fo, Gn, and Ag

Note: *n*, number of examined fluid inclusions. Fluid inclusions: (p) primary, (p–s) primary–secondary, (s) secondary. Minerals: (An) anhydrite; (Ba) barite; (Q) quartz; (Car) carbonate; (Ag) native silver; (Au) native gold; (Bi-ss) Bi sulfosalts; (Fo) fahlore; (Bour) bournonite; (Cp) chalcopyrite; (Gn) galena; (Py) pyrite; (Sn-ss) Cu–Fe sulfostannates; (Tdm) tetradymite.
* Fluid boiling.

mately similar T_{hom} values (254–130°C, averaging 200°C at $n = 58$) are determined for fluid inclusions from quartz and barite representing mineralization of the post-productive stage. Estimates of the pressure under which ores of the main productive stage formed vary from 27–12 bar at upper levels to 90–65 bar at the lower levels (Table 7). It is noteworthy that the temperature values (275–200°C, averaging 235°C at $n = 33$) determined for fluid inclusions from quartz of ore body 26 in the Pervaya zone are intermediate between T_{hom} estimates for mineralization of the early and main productive stages of the Diabazovaya zone mineralization. Simultaneously, pressure estimates (25–20 bar; sample 136/87, Table 7) for fluids from the Pervaya zone are very close to the values determined for mineralization developed at the upper level of the Diabazovaya zone (27–12 bar; sample 65/82, Table 7).

The data in Table 7 represent minimal temperature estimates of mineral growth. Nevertheless, since fluid boiling was established for inclusions from both the upper and the lower parts of the ore zone, the measured T_{hom}, including maximum values, do not require correction for pressure because *P–T* conditions were likely close to two-phase (liquid–vapor) boiling parameters corresponding to the hydrostatic regime (Roedder, 1984). Thus, the obtained T_{hom} estimates can be considered to be close to entrapment temperatures.

The wide development of hydrothermal ore breccia throughout the entire vertical interval of the Diabazovaya zone, particularly intense in areas of high-grade ores, demonstrates that productive mineral associations of the main ore stage formed under conditions of fluid boiling that was caused by sharp changes in the *PT* regime due to intermittent explosive release of excessive pressure in the system (Fournier, 1985; Nelson and Giles, 1985). The low-salinity fluid (up to 6 wt %-equiv NaCl) begins boiling at a temperature of 200–250°C at a depth of about 400 m, which corresponds to a hydrostatic pressure of ~30 bar (Haas, 1971). This depth seems quite realistic for the supposed setting of the recovered level of the deposit and is in agreement with obtained pressure estimates for ore samples from upper levels of the deposit (adits 1, 9; Table 7). Unexpectedly high pressure values (120 bars) were obtained for sample 64/82, which was also taken at the level of adit 1, but characterizes the early ore-free association. Under such pressure in a high-temperature (>300°C) vapor-dominated hydrothermal system functioning under hydrostatic conditions, fluid can start boiling at depths exceeding 800 m, a process which, in addition, strongly varies depending on the quantity of CO_2 dissolved in the fluid (Hedenquist and Henley, 1985; Nelson and Giles, 1985). This suggests that the early hydrothermal mineralization of the Kairagach deposit could form at deeper levels than most of the productive gold-bearing epithermal mineralizations.

Concentrations of salts in fluids from primary and primary–secondary fluid inclusions vary within a wide range (Table 7). Mineral-forming fluids of the early gold–pyrite–quartz mineralization are characterized by relatively low (from 4.9 to 0.5 wt %, averaging 1.8 wt %-equiv NaCl at $n = 114$) salinity. Similar salt concentrations (5.0–0.7 wt %, averaging 2.4 wt %-equiv NaCl at $n = 33$) are established for fluids characterizing the gold–silver–quartz mineralization of the Pervaya zone. Higher values and their wider variations are determined for fluid inclusions from minerals of the gold–fahlore–sulfosalt–telluride mineralization corresponding to the main productive stage (13.4–0.9 wt %, averaging 6.0 wt %-equiv NaCl at $n = 66$) and from the gold-free quartz–carbonate–barite veins and stringers associated with galena, sphalerite, and chalcopyrite that characterize the post-productive stage (14.6–5.7 wt %, averaging 12.4 wt %-equiv NaCl at $n = 53$).

The measured eutectic temperatures (Table 7; Fig. 13) indicate the chloride composition of fluid from inclusions and variable concentrations of Ca, Na, K, and Fe ions (temperature intervals of –55 to –41°C and –36 to –17, 12°C; Borisenko, 1977). Combined with the data on changes in fluid salinity, this suggests that the hydrothermal system of the Kairagach deposit was fed from several different fluid sources. Nevertheless, when the T_{eut} values obtained for secondary fluid inclusions, ranging mainly from –55 to –36°C, are excluded from consideration, it appears (Table 7) that fluid inclusions from minerals of ore stages in both ore zones are characterized by close composition of chloride solutions with variable proportions of dominant Na and K (T_{eut} from –28 to –12°C; Borisenko, 1977). Observed variations in the composition of the mineral-forming solution most likely resulted from its evolution during ore formation, since no noticeable signs of an inverse linear relationship between the salinity of the solution and its temperature, which is usually considered as evidence for mixing of different-type solutions, are registered (Fig. 13). Simultaneously, the distribution in the diagram of data points corresponding to primary fluid inclusions from minerals of the main productive stage indicates a substantial increase in salt concentration with the temperature drop (approximately, from 5 to 10 wt %-equiv NaCl). Such a trend is usually interpreted as resulting either from removal of vapor-forming H_2O and other volatiles during fluid boiling or from involvement of more concentrated but less heated solutions in the hydrothermal system (Roedder, 1984).

INVESTIGATIONS OF STABLE ISOTOPES

Stable isotopes in minerals of ores and altered host rocks provide information about sources for some elements and fluids, as well as about ore-forming conditions (Ohmoto, 1972; Taylor, 1979). We studied the isotopic composition of S in sulfides and sulfates; O in quartz, sulfates, and sericites; and C in carbonates, characterizing mainly the hydrothermal mineralization of the Diabazovaya and, partly, Pervaya zones. Determinations of S, O, and C isotopes in minerals were per-

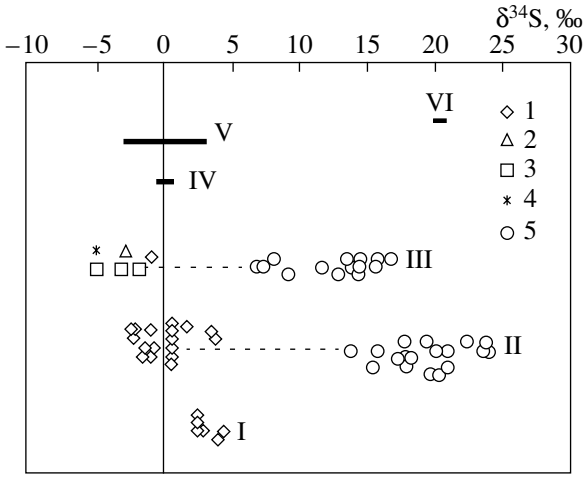

Fig. 14. Isotope composition of S in minerals of the Kairagach deposit and in main natural reservoirs: (I) altered andesites; (II) early and main productive stages; (III) post-productive stage; (IV) meteoric S; (V) magmatic water; (VI) sea sulfate S; (1) pyrite; (2) galena; (3) chalcopyrite; (4) sphalerite; (5) barite.

formed by L.P. Nosik (Institute of Geology of Ore Deposits, Petrography, Mineralogy, and Geochemistry (IGEM)) following the procedure described in (Nosik, 1986). The O and H isotope compositions of the OH group were studied earlier by B.G. Pokrovskii in three sericite samples (Kovalenker *et al.*, 1994). Table 8 demonstrates the results of isotope studies.

Sulfur Isotopes

The data obtained show the relatively narrow (from –5.10 to +4.64‰, averaging +0.11‰ at $n = 30$) range of variations in the S isotope composition in sulfides and the wider (from +6.98 to +24.25‰, averaging +15.80‰ at $n = 46$) variations of $\delta^{34}S$ in sulfates (Fig. 14). For comparison, intervals of variations in the S isotope composition in main natural reservoirs are also shown in the diagram.

Minimal $\delta^{34}S$ values are characteristic of galena, sphalerite, and chalcopyrite from quartz–carbonate–barite veins and stringers of the post-productive stage (–5.10 to –0.85‰, averaging –3.17‰ at $n = 6$) and maximum estimates were obtained for pyrites from altered (quartz–sericite–carbonate type) andesites (+2.57 to +4.64‰, averaging +3.31‰ at $n = 6$). In pyrites of the early and main productive stages, the $\delta^{34}S$ values vary from –2.39 to +3.94‰ (averaging +0.15‰ at $n = 18$). Sulfates of the productive and post-productive stages differ in S isotope composition (Fig. 14). The $\delta^{34}S$ values in barites from the productive stage vary from +13.96 to +24.25 ‰ (averaging +19.26‰ at $n = 19$); these values in barites of the post-productive stage range from +6.98 to +16.96‰ (averaging +12.71‰ at $n = 15$). These values are similar to those obtained for sulfides and sulfates of the Kochbulak deposit (Kovalenker *et al.*, 1997) and correspond, in general, to the variations in other epithermal deposits of precious metals (Field and Fifarek, 1985).

The relatively narrow range of variation of $\delta^{34}S$ in sulfides and the substantial enrichment of sulfates with heavy S isotopes with the temperature decrease noted in the Kairagach deposit (Tables 7, 8; Fig. 14) indicate that the reduced S form (H_2S) in the mineral-forming solution prevailed over the oxidized one (Ohmoto, 1986; Rye, 1993). In this case, the integral isotope composition of the fluid approximates $\delta^{34}S$ values of H_2S.

The $\delta^{34}S$ values in H_2S of fluid that is in equilibrium with pyrites of productive stages and calculated for the temperature 250°C (Ohmoto and Rye, 1979) range from –2.39 to +3.61‰ (average +0.21‰), and those in H_2S of fluid balanced with sulfides of the post-productive stage at a temperature of 200°C range from –4.88 to +0.87‰ (average +0.87‰). Such $\delta^{34}S$ values are traditionally referred to the magmatic source of sulfur (0 ± 5‰; Ohmoto, 1986). This implies that S from mineral-forming solutions of the Kairagach deposit is mainly magmatic in origin, similarly to most other epithermal deposits (Henley, 1991).

The calculated $\delta^{34}S$ values in H_2S of fluid in equilibrium with barites show significant variation, from –10.23 to +0.06‰ (average –4.93‰) for productive barites at a temperature of 250°C and from –22.47 to –12.49‰ (average –16.74‰) for post-productive barites at 200°C, which conflicts with the data on sulfides. This discrepancy can be explained by different factors. First, isotopic equilibrium between the reduced and oxidized S forms in fluid either was never reached or was disturbed due to fluid boiling. Second, the f_{O_2} increase in fluid due to the influx of oxygen-saturated meteoric water into the hydrothermal system could result in partial oxidation of sulfur in H_2S (Ohmoto, 1986).

S isotope thermometry was used in this study only once, when we succeeded in determining the S isotope composition in co-occurring pyrite and barite from sulfide–quartz–barite stringers of the post-productive stage (sample Kai-22, Table 8). The calculated temperature value estimated with the partition equation for balanced pyrite and barite (Field and Fifarek, 1985) is 248°C and occurs within the temperature interval of 254–200°C, characteristic of this mineralization.

Carbon Isotopes

The $\delta^{13}C$ values in six samples of carbonates from stringers in hydrothermally altered (quartz–sericite–carbonate type) host andesite–porphyry vary, relative to the PDB standard (Table 8), from –4.10 to –0.62‰ (averaging –2.1‰ at $n = 6$). Under the physicochemical parameters of epithermal ore formation, when carbon in fluid is mostly represented either by carbon dioxide dissolved in water or as H_2CO_3, differences between the isotope composition of carbonate C and equilibrated

Table 8. Isotope composition of S, O, H, and C in hydrothermal minerals of the Kairagach deposit

Horizon of the adit, m	Sample number	$\delta^{34}S$, ‰		$\delta^{18}O$, ‰				δD, ‰	$\delta^{13}C$, ‰	Note
		Py (Cp, Gn, Sp)	Ba (An, Gs)	Q	Ba (An, Gs)	Ser	Car	Ser	Car	
5 (+1400)	8/86	(–5.00; Gn)								Gn–Ba stringer in diabase–porphyry dike
	10/86	(–1.95; Gn)	7.49		–0.56; –0.74					
	522/83			4.82						Quartzite
1 (+1350)	22/82	–0.85 (–5.10; Cp)	8.26	11.05	2.20					Gold-free Py–Cp–Ba–Q vein
	64/82			3.39						Early gold-free Q
	1049/82			10.39; 9.69						Ore-free Q with Py and Fo
7 (+1300)	159/198				(11.78 10.98; Gs)					Gs stringer in andesite–porphyry
	553/87		15.57			.				Ore-bearing Ba
	554/87					0.80		–63		Q-Ser alteration
9 (+1300) (Pervaya zone)	148/87	(–3.12; Gn) (–2.98; Sp)	13.62		2.65; 2.64					Sp–Gn–Ba vein crosses the structure of ore body 26 of the Pervaya zone
4 (+1250)	90/84			8.12						Early ore-bearing Q
	5/85		11.75		1.47					Quartzite with Py, Fo, and Ba nests
	24/85		17.77		6.55					Ore-bearing Ba
	25/85				2.49					
	42/85		23.60; 24.00		1.22; 0.83					
	444/86				–1.75					
3 + 40 (+1140)	1074/86		19.51 (13.64; An)		9.99, (8.83; An)					Ba and An accumulations in ore body
	24/91		6.98		13.97					Ba stringer in andesite–porphyry
	27/91		9.22		13.59					
	28/91		(17.19; Gs)		(5.94; Gs)					″ Gs
3 + 40 (+1140)	38/91		16.96		7.01					″ Ba
	40/91		(12.62; Gs)		(6.12; Gs)					″ Gs in andesite
	51/91		14.00		10.79					Gn–Ga stringer
	53/91		19.82	4.51	1.64					Ba nest-shaped accumulations in quartzite
	56/91		17.87		11.23					

Table 8. (Contd.)

Horizon of the adit, m	Sample number	$\delta^{34}S$, ‰		$\delta^{18}O$, ‰				δD, ‰	$\delta^{13}C$, ‰	Note
		Py (Cp, Gn, Sp)	Ba (An, Gs)	Q	Ba (An, Gs)	Ser	Car	Ser	Car	
	57/91		21.17		9.58					
	140/91		14.59							White coarse-grained Ba
	144/91	0.72								Silicified andesite–porphyry with sulfide dissemination
	148/91	0.72								
	150/91	3.94								
	152/91		(13.04; Gs)		(5.12; Gs)					Gs stringer in andesite
	153/91	–1.23								Quartzite
3 (+1100)	36/86				1.14					Ore-bearing Ba
	67/86		22.57		0.53					
	68/86		24.25		–0.41					
	368/86		12.92							Post-ore Ba
	1073/86		20.22		1.74, 0.60					Minerals of the main productive stage and Gs stringers in quartzite
	127/87		13.96		5.25/4.91					
	543/87		17.33 (18.80; An)		6.42					
	545/87	1.72	(15.43; Gs)							
	51/87		22.57							
	9/88	0.72	(13.51; An)		(9.49; An)	2.30		–68		
	11/88	3.61	(15.51; Gs)		7.42 (11.93; Gs)					Ba, An, Ser, and sulfide accumulations and crossing Gs stringers in aggregates of the main productive stage within quartzite
	B-25/88					5.4		–59		
	108/89			0.47		12.90				
	1239/90		(17.19; An)		(10.99; An)					
	26/91	2.67								Silicification zone
3 (+1100)	30/91	0.72								Q–Ser alteration
	42/91	0.72								
	46/91	2.72								″

Table 8. (Contd.)

Horizon of the adit, m	Sample number	$\delta^{34}S$, ‰		$\delta^{18}O$, ‰				δD, ‰	$\delta^{13}C$, ‰	Note
		Py (Cp, Gn, Sp)	Ba (An, Gs)	Q	Ba (An, Gs)	Ser	Car	Ser	Car	
	144/91	0.72								Q–Ser alteration
	148/91	0.72								
	150-b/91	3.94								Quartzite
12 + 25 (+1025)	Kai-21/1		14.45		11.46					Pink–gray Ba + An aggregates
	Kai-21/2		15.85		11.86					
	Kai-22/1		15.72		8.96					Coarse-grained Ba
	Kai-22/2		14.38, 14.46		8.59					
	Kai-23	–2.39	20.50		11.10					Ba–An–Gs aggregate within quartzite
12 (+1000)	Kai-12			8.50, 8.91						Quartzite
	Kai-31	–2.17				8.16				
	Kai-34		18.17, 18.48	11.44	9.11, 10.11					Q–Ba–An aggregate with Au
	Kai-41					9.01				Ser in Au–Te–Q–Ba aggregate
	Kai-43	–2.10	13.97	10.50	10.76					Q–Ba aggregate with Au, Fo, and tellurides
Borehole 1001	74/91	0.72								Quartzite
	1185/90a						9.82		–4.10	Stringer of white Car
	1185/90b						13.99		–2.58	Stringer of pink Car
Borehole 1004	1213/90	4.64								Beresite
	1215/90	3.09								Altered andesite
	1216/90						25.00		–2.01	Stringer of white Car
	1219/90	2.57								Altered andesite
	1219·/90	4.14								
	1220/90						13.60		–0.62	Stringer of white Car
	1229/90						15.94		–2.55	Stringer of pink Car
	1230/90	0.72								Quartzite
	1232/90						15.59		–0.99	Stringer of pink Car

Note: Minerals: (An) anhydrite; (Gs) gypsum; (Ba) barite; (Fo) fahlore; (Car) carbonate; (Cp) chalcopyrite; (Gn) galena; (Py) pyrite; (Ser) sericite; (Sp) sphalerite.

fluid are below 1‰ (Field and Fifarek, 1985; Ohmoto, 1986). Thus, the interval of variations of $\delta^{13}C$ values in carbonates is close to the interval in their parent solutions, which record variations in the isotope composition of the primary source. The $\delta^{13}C$ values measured in carbonates from altered host rocks of the Kairagach deposit are between values characteristic of magmatic rocks that were melted from the mantle source (-5 ± 2‰) and marine limestones (0 ± 4‰; Ohmoto and Rye, 1979). This suggests that the C source in fluids that were responsible for quartz–carbonate–sericite alteration of host andesites is likely mixed, or juvenile–crustal, in origin.

Oxygen and Hydrogen Isotopes

Table 8 displays data on oxygen isotope composition measured in quartz, sericite, barite, gypsum, anhydrite, and carbonates (13, 6, 35, 8, 3, and 6 samples, respectively) representing different-age associations of hydrothermal minerals distributed in the ore zones of the Kairagach deposit. The δD values obtained earlier for three sericite samples (554/87, 9/88, and 1185/90a) from ore bodies of the Diabazovaya zone (Kovalenker *et al.*, 1994) are also shown in this table.

The $\delta^{18}O$ values are characterized by a significant scatter (relative to SMOW) with the minimal value (+0.47–4.82‰, averaging +3.3‰ at $n = 4$) measured in early high-temperature quartz from veins and quartzites unbounded with gold-productive stages proper (samples 64/82, 108/89, 53/91, and 522/83). Quartz from productive associations is usually characterized by higher contents of heavy oxygen isotope and relatively low variations (+8.12–+11.44‰, averaging +9.65‰ at $n = 7$). Presumed $\delta^{18}O$ values of the fluid in equilibrium with quartz from post-ore and gold-productive associations and calculated, using the known equations of isotope fractionation (Matsuhisa *et al.*, 1979), for temperatures of 300 and 250°C are within the ranges of –6.39 to –2.04‰ (average –3.57‰) and –0.78 to +2.52‰ (average +0.75‰), respectively.

The oxygen isotope composition in barites from mineral associations of the main productive and post-productive stages is highly variable, but shows no substantial differences between them: the $\delta^{18}O$ values range from –1.75 to +11.23‰ (averaging +5.22‰ at $n = 23$) in the former stage and from –0.74 to +13.97‰ (averaging +7.02‰ at $n = 13$) in the latter. The similarity of isotopic characteristics is probably explained by very close temperature intervals of barite formation in these associations, as was shown above. The $\delta^{18}O$ values in H_2O of the fluid equilibrated with barites of the productive and post-productive stages, calculated with the fractionation equation (Friedman and O'Neil, 1977) for a temperature of 200°C, vary from –8.37 to +4.61‰ (average –1.4‰) and from –7.36 to +7.35‰ (average +0.40‰), respectively. The oxygen isotope composition in gypsum and anhydrite (–4.81 to +11.78‰, averaging +5.55‰ at $n = 11$) is noticeably enriched in $\delta^{18}O$, although within the variation range of heavy oxygen isotope in barites from the post-productive stage. At a temperature of 150°C, accepted for the formation of gypsum and anhydrite, calculated $\delta^{18}O$ values of H_2O in fluids equilibrated with these minerals should vary from –23.59 to –6.85‰ (average –13.24‰).

The $\delta^{18}O$ values in carbonates from altered (quartz–sericite–carbonate type) andesite–porphyries vary from +9.82 to +25.00‰. With the formation temperature of these carbonates taken as 200°C, presumed $\delta^{18}O$ values of H_2O in fluids equilibrated with these carbonates that are calculated using the corresponding fractionation factor (Friedman and O'Neil, 1977) should vary from –0.28 to +15.46‰.

Sericites from the Diabazovaya ore zone are characterized by significant variations in the $\delta^{18}O$ value: from +0.80‰ in the zone of quartz–sericite alteration and +2.3…+5.3‰ in the early gold–pyrite–quartz association to +8.16–+12.90‰ in gold-bearing quartz–barite associations of the main productive stage. Variations in δD values are very low, from –68 to –59‰ (SMOW). If one takes into consideration that the partition factor of hydrogen isotopes between muscovite (sericite) and balanced H_2O under formation temperatures of ore mineralization is close to zero in this zone (Bowers and Taylor, 1985), the obtained δD values can probably be considered as characterizing H_2O from the mineral-forming fluid responsible for formation of gold–sulfide–selenide–telluride ores of the Kairagach deposit. Simultaneously, the estimates of the oxygen isotope composition of H_2O from fluids calculated, using the equation of oxygen isotope partition between muscovite and water (Friedman and O'Neil, 1977) and available data on sericites, for a temperature of 250°C, show changes in $\delta^{18}O$ values in H_2O of fluid from –4.2‰ in the zone of quartz–sericite wall rock alterations to –2.7…+0.3‰ in ores of the early productive stage and to +3.2 …+7.9‰ in ores of the main productive stage.

WATER SOURCES OF ORE-FORMING SOLUTION

According to calculations for sericite, quartz, and barite, the isotope composition of the mineral-forming fluid responsible for deposition of ores in the Kairagach deposit corresponds to the following range of values: $\delta D = -68$ to –59‰ and $\delta^{18}O = -8.37…+7.90$‰. These data are shown in Fig. 15, which also includes data on meteoric water (LMW; Taylor, 1979) and the isotopic composition of primary magmatic water (PMW; Taylor, 1979) and seawater (SMOW), as well as data (Chernov and Sultanzhodzhaev, 1989) on present-day surface water ($\delta D = -94$ to –62‰, averaging –80‰; $\delta^{18}O = -13…-9$‰, averaging –11.25‰) and buried water from Paleozoic rocks ($\delta D = -80$‰; $\delta^{18}O = -9.8…+8.1$‰) of the Tashkent region. The buried water is, probably, meteoric water that experienced an insignificant isotopic shift.

The variation range of δD in H_2O of the mineral-forming fluid from the Kairagach deposit corresponds to the average isotopic composition of H in the PMW; nevertheless, the $\delta^{18}O$ values vary from those characteristic of buried water from Paleozoic rocks of the Tashkent region to the average value of the PMW (Fig. 15). Such isotopic composition of H_2O of the presumed mineral-forming solution suggests that waters of magmatic and meteoric origin are its main constituents. Simultaneously, since all δD values and most of the $\delta^{18}O$ values in H_2O of the mineral-forming solution appear to be localized within or near the PMW composition area (Fig. 15), it is possible that composition of the ore-forming fluid was dominated by a magmatic component. Such an assumption is also supported by the data mentioned above on the magmatic origin of sulfur, as well as by the data on fluid inclusions, according to which F of undoubtedly juvenile origin played an important role in fluid composition.

The enrichment of the H_2O composition with heavy oxygen isotope could, however, be caused by fluid boiling. In addition, a significant share of $\delta^{18}O$ estimates in the presumed isotopic composition of H_2O falls within the area of negative values (Fig. 15) characteristic of meteoric water modified due to interaction with host rocks (Taylor, 1979). We believe, therefore, that meteoric water also played a substantial role in production of the ore-forming solution.

To substantiate this conclusion and estimate the share of different water sources, we carried out, using a known approach (Ohmoto and Rye, 1974), modeling of the probable composition of the ore-forming solution in the Kairagach deposit. When calculating the mass balance, we assumed that the $\delta^{18}O$ = +7.5‰ and δD = –62.5‰ values correspond to the initial PMW composition and average $\delta^{18}O$ (–9.0‰) and δD (–80‰) values of local meteoric water, to meteoric water. The averaged values ($\delta^{18}O$ = +7‰ and δD = –70‰) available for intermediate–acid volcanogenic rocks (Field and Fifarek, 1985) were used for characterizing the isotopic composition of host rocks. Calculations were performed for temperatures of 200, 250, and 300°C and w/r ratios equal to 1.0, 0.1, and 0.01. It appeared (Fig. 15) that calculated variations in the H_2O isotope composition under these parameters make it possible that both local meteoric and magmatic waters interacted with magmatic rocks. Under conditions of a w/r ratio ranging from 0.01 to 0.1 and a temperature of 300°C, magmatic water could be a main factor in formation of the mineral-forming fluid, whereas at lower temperatures, meteoric water could play this role.

Thus, a combination of the isotopic data mentioned above and theoretical modeling of the probable composition of the mineral-forming solution allows us to conclude that the fluid responsible for the gold–sulfide–selenide–telluride mineralization of the Kairagach deposit represented a mixture of magmatic and meteoric waters with modified initial composition due to their interaction with host rocks.

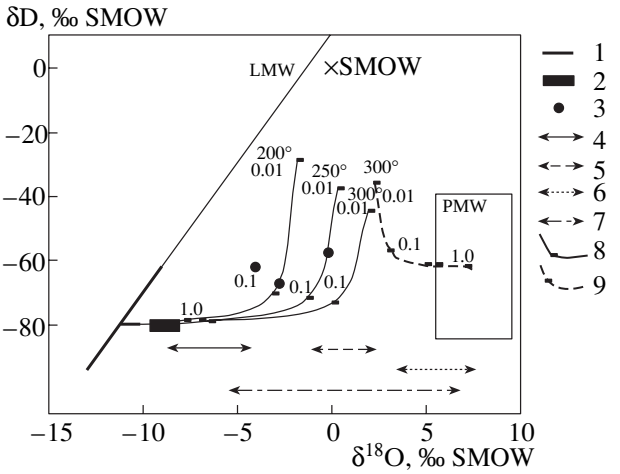

Fig. 15. Comparison of calculated H_2O δD and $\delta^{18}O$ values of the ore-forming fluid in the Kairagach deposit with isotopic characteristics of main hydrosphere reservoirs. PMW, primary magmatic water; LMW, line of meteoric water; SMOW, seawater. (1, 2) Present-day meteoric (1) and buried (2) water from Paleozoic formations of the Tashkent region; (3) water in equilibrium with sericites of the deposit; (4–7) variation intervals of $\delta^{18}O$ in water occurring in equilibrium with minerals of the deposit at T = 250°C: (4) with quartz of the early productive stage, (5) with quartz of the main productive stage, (6) with sericite of the main productive stage, and (7) with barite of the main productive stage; (8, 9) model variations of the δD and $\delta^{18}O$ values in meteoric (8) and magmatic (9) water in the course of interaction with volcanogenic host rocks at different temperatures and water–rock proportions (w/r).

GOLD OCCURRENCE FORMS AND CONCENTRATION IN MINERAL-FORMING SOLUTION

The data discussed above on physicochemical parameters and composition of the mineral fluid in the Kairagach deposit were used to define probable gold occurrence forms and assess gold concentrations depending on variations in the solution temperature. With this object in view, we performed thermodynamic modeling of the balanced gold solubility in the Au–NaCl–CO_2–H_2S–H_2O system. We used the program GIBBS version 3.6 with the thermodynamic data bank UNITERM version 3.6 (Shvarov, 1992). Temperature and pressure intervals, as well as the initial composition of the system for the assessment of the temperature dependence of the balanced solubility of gold (taken in excess), were selected with account of the results obtained in the course of the study of fluid inclusions: 1 kg H_2O, 1 M NaCl, 0.06 M CO_2, 0.08 M H_2S, 0.02 M SO_2, and 1 M Au.

Figure 16 demonstrates that Au occurrence forms and solubility strongly depend on changes in the temperature, pH, and Eh of the model fluid. Gold occurs in

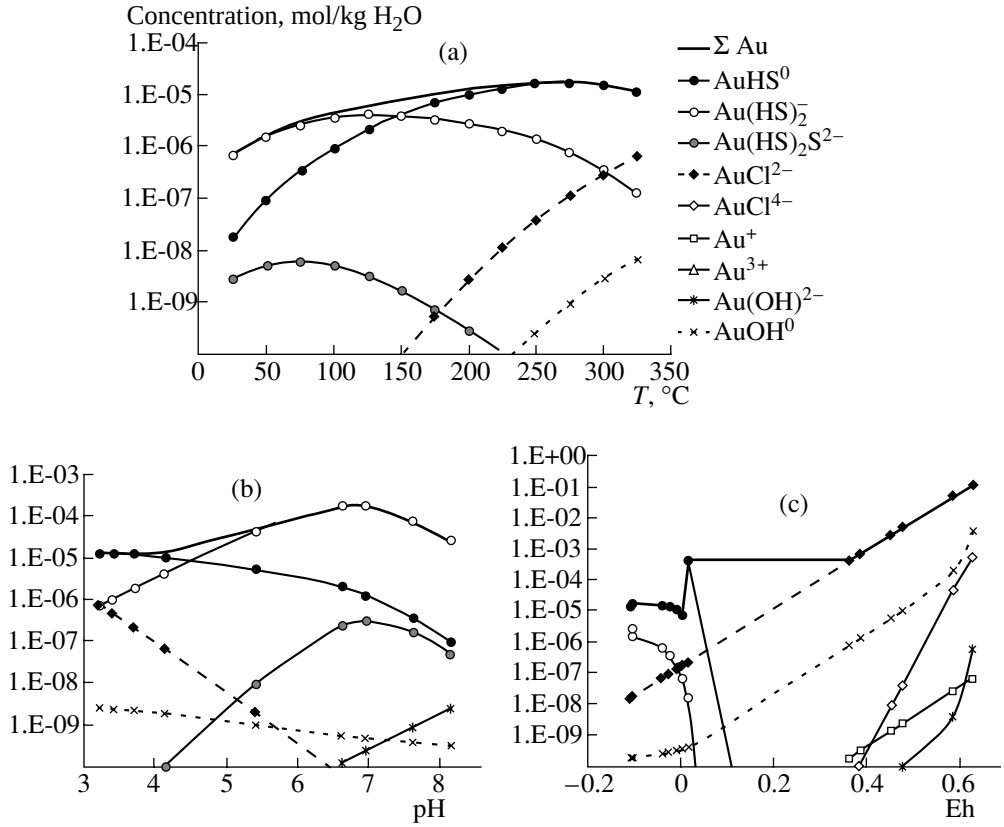

Fig. 16. Solubility of different gold complexes and dependence on the temperature (a), pH (b), and Eh (c), according to thermodynamic modeling.

solution mainly in the form of $AuHS^0$ and $Au(HS)_2^-$ complexes, whereas the share of other forms, such as Au^+, Au^{3+}, AuOH, $Au(OH)^{2-}$, $Au_2(HS)_2S^{2-}$, $AuCl_2^-$, and $AuCl_4^-$, is negligible. In the temperature interval of 350–175°C, the $AuHS^0$ complex is prevalent in the solution and composes up to 90% of all gold dissolved in the particular solution, whereas the $Au(HS)_2^-$ complex dominates the solution under lower temperatures, i.e., <150°C (Fig. 16a). At temperatures of 250°C and lower, total Au solubility sharply decreases, which stimulates Au precipitation from the solution.

The dependence of Au solubility on variations in acidity–alkalinity of the solution was calculated in the interval of pH values ranging from 3 to 8 (Fig. 16b). It was established that, at pH 3–4, the solution is dominated by the $AuHS^0$ complex, and the Au content is about 1×10^{-5} mol/kg H_2O, remaining stable. The rise of pH up to 6.5 (for instance, because of removal of acid gases due to fluid boiling) results in the increase of Au solubility by more than ten times, and its content increases up to 1.6×10^{-4} mol/kg H_2O. A further increase in solution alkalinity (up to pH 8) results in a reduction in Au solubility up to the initial value. The $Au(HS)_2^-$ complex represents the main Au occurrence form in solutions with pH exceeding 4.5.

The influence of the oxidizing potential (Eh) on Au solubility was estimated for H_2S/SO_2 values ranging from 0.1 to 1.0. The obtained estimates (Fig. 16c) show that changes in the Eh of the solution from 0.3 ($H_2S/SO_2 = 0.1$) to –0.01 ($H_2S/SO_2 = 0.6$) result in the decrease of the Au concentration by four orders of magnitude, from 10^{-1} to 10^{-5}. A further Eh decrease up to −1.2 ($H_2S/SO_2 = 10$) does not cause any noticeable changes in solubility. In a solution with the Eh amounting to 0.005 ($H_2S/SO_2 = 0.4$), chlorides ($AuCl_2^-$ and $AuCl_4^-$) and hydroxides ($AuOH^0$) are prevalent, while $AuOH^0$ dominates in other cases.

In line with the mineralogical–geochemical zoning and S isotope data mentioned above, the mineral formation environments in the Kairagach deposit changed from relatively reducing ($H_2S > SO_2$, Eh < 0) at deeper levels to highly oxidizing (Te^{4+} in goldfieldite) upward. The results of thermodynamic calculations point to an increase in Au solubility with an elevation in Eh in the model solution (Fig. 16c). Probably, this explains the decrease in the Au content in ores formed in more oxi-

dizing settings, i.e., toward the upper levels of the deposit.

The results of modeling allow us to conclude that most of the gold precipitated from the solution due to decomposition of the $AuHS^0$ complex within the temperature interval of 250–125°C, which corresponds to the formation temperatures of gold–sulfide–selenide–telluride–quartz–barite mineral associations of the main productive stage. Gold-impoverished associations of the earlier productive stage formed mainly because of decomposition of the $Au(HS)_2^-$ and, partly, $AuCl_2^-$ complexes under the relatively high temperatures (300–250°C) corresponding to the temperature regime of this stage. The data obtained suggest that cooling of the mineral-forming solution was one of the main factors responsible for precipitation of gold in the course of productive mineralization in the Kairagach deposit. Such cooling could be caused by the fluid cooling away from the heat source; boiling in response to the pressure fall; and, finally, mixing with colder underground waters. As was shown in different sections of this paper, all these mechanisms functioned in the course of ore formation in the Kairagach deposit.

Simultaneously, according to the analysis of mineral parageneses, mineralization of the early productive stage, as well as earlier mineral associations of the main productive stage, formed in acid environments (under pH 2–4), whereas later associations of this stage formed in slightly acid to neutral settings. The increase in Au solubility under elevated pH in the model solution explains the fact that gold enriches mainly mineralization of the main productive stage, which formed under moderate pH values.

ACKNOWLEDGMENTS

We express our gratitude to L.P. Nosik and B.G. Pokrovskii, who performed isotope analysis; A.I. Tsepin for the microprobe study of mineral composition; and V.R. Heinke and T.R. Khalmukhamedov for their assistance in collecting geological materials. The work was supported by the Russian Foundation for Basic Research (project nos. 01-05-64081, 02-05-06196 MAS, and 01-05-64675).

REFERENCES

Badalov, A.S. and Spiridonov, E.M., Fahlores and Native Gold of the Kairagach Occurrence (Eastern Uzbekistan), *Uzb. Geol. Zh.*, 1983, no. 2, pp. 74–78.

Badalov, A.S., Spiridonov, E.M., Heinke, V.P., and Pavshukov, V.V., Minerals–Native Elements and Tellurides of the Kairagach Volcanic Occurrence (Uzbek Soviet Socialist Republic), *Zap. Uzb. Otd. Vses. Miner. O–va*, 1984, no. 37, pp. 64–67.

Bodnar, R.J. and Vityk, M.O., Interpretation of Microthermometric Data for H_2O–NaCl Fluid Inclusions, *Fluid Inclusions in Minerals: Methods and Applications: Short Course of the Working Group "Inclusions in Minerals,"* Pontignano-Siena: Virginia Tech, 1994, pp. 117–130.

Bonham, H.F., Jr., Models for Volcanic-Hosted Epithermal Precious Metal Deposits: a Review, *Int. Volcanol. Congress. Symp. 5. Proceedings*, Hamilton (New Zealand), 1986, pp. 13–17.

Borisenko, A.S., The Study of Salt Composition of Gas–Liquid Inclusions in Minerals by the Cryoscopy Method, *Geol. Geofiz.*, 1977, no. 8, pp. 16–27.

Bowers, T.S. and Taylor, H.P., Jr., An Integrated Chemical and Stable Isotope Model of the Origin of Midocean Ridge Hot Spring Systems, *J. Geophys. Res.*, 1985, vol. 90, pp. 12583–12606.

Brown, P.E., FLINCOR: A Fluid Inclusion Data Reduction and Exploration Program, *Second Biennial Pan-American Conference on Research on Fluid Inclusions*, Blackburn: Virginia Tech, 1989, p. 14.

Chernov, I.G. and Sultanzhodzhaev, A.A., The Complex Study of Isotopic Composition of Underground Waters in Tashkent Artesian Basin, *Tezisy dokladov XII Vsesoyuz. simpoziuma po stabil'nym izotopam v geokhimii* (Abstracts of Papers of XII All-Union Symp. on Stable Isotopes in Geochemistry), Moscow: Vernadsky Inst. Geokhim. Analit. Khim., 1989, p. 174.

Cunningham, C.G., Characteristic of Boiling-Water-Table and Carbon Dioxide Models for Epithermal Gold Deposition, *Geologic Characteristics of Sediment- and Volcanic-Hosted Disseminated Gold Deposits–Search for An Occurrence Model. USGS Bull.*, 1985, no. 1646, pp. 43–46.

Field, C.W. and Fifarek, R.H., Light Stable-Isotope Systematic in the Epithermal Environments, *Rev. Econ. Geol.*, 1985, vol. 2, pp. 99–128.

Fournier, R.O., The Behavior of Silica in Hydrothermal Solutions, *Rev. Econ. Geol.*, 1985, vol. 2, pp. 45–61.

Friedman, I. and O'Neil, J.R., Compilation of Stable Isotope Fractionation Factors of Geochemical Interest, *U.S.G.S. Prof. Paper*, 1977, no. 440-kk.

Haas, J.L., Jr., The Effect of Salinity on the Maximum Thermal Gradient of a Hydrothermal System at Hydrostatic Pressure, *Econ. Geol.*, 1971, vol. 66, pp. 940–946.

Heald, P., Foley, N.K., and Hayba, D.O., Comparative Anatomy of Volcanic-Hosted Epithermal Deposits: Acid–Sulfate and Adularia-Sericite Types, *Econ. Geol.*, 1987, vol. 82, no. 1, pp. 1–26.

Hedenquist, J.W. and Henley, R.W., Effect of CO_2 on Freezing Point Depression Measurements for Epithermal Ore Deposition, *Econ. Geol.*, 1985, vol. 80, no. 5, pp. 1379–1406.

Henley, R.W., Epithermal Gold Deposits in Volcanic Terranes, *Gold Metallogeny and Exploration*, Glasgow: Blackie, 1991, pp. 133–164.

Islamov, F., Kremenetsky, A., Minzer, E., and Koneev, R., The Kochbulak–Kairagach Ore Field, Au, Ag, *and* Cu *Deposits of Uzbekistan. Excursion Guidebook*, Potsdam: GFZ, 1999, pp. 91–106.

Koneev, R.I. and Gertman, Yu.L., Microparageneses of Gold in Gold-Ore Formations of Eastern Uzbekistan, *Osnovnye problemy v uchenii o magmatogennykh rudnykh mestorozhdeniyakh* (Principle Problems in the Science on Magmatic Ore Deposits), Moscow: Inst. Geol. Rudn. Mest. Ross. Akad. Nauk, 1997, pp. 142–143.

Kovalenker, V.A., Typomorphic Minerals of Ores from Shallow Gold–Silver Deposits of the Upper Paleozoic Volcanic

Region in Central Asia, *Metasomatizm, mineralogiya i voprosy genezisa zolotykh i serebryanykh mestorozhdenii v vulkanicheskikh tolshchakh* (Metasomatism, Mineralogy, and Problems of Genesis of Gold and Silver Deposits in Volcanic Rocks), Moscow: Nauka, 1986, pp. 111–145.

Kovalenker, V.A. and Heinke, V.P., New Cu–Sn–Bi–Se Type of Mineralization in Kuramin Subzone of the Central Tian Shan, *Izv. Akad. Nauk SSSR, Ser. Geol.*, 1984, no. 5, pp. 91–104.

Kovalenker, V.A., Nekrasov, I.Ya., and Malov, V.S., Mineralogy and Parageneses of Cu and Fe Sulfostannates in Gold–Silver Deposits, *Geol. Rudn. Mestorozhd.*, 1986, no. 2, pp. 67–84.

Kovalenker, V.A., Trubkin, I.V., and Malov, V.S., Hodrushite, $Cu_8Bi_{12}S_{22}$: First Finding in the Soviet Union, *Novye dannye o mineralakh* (New Data on Minerals), Moscow: Nauka, 1987, issue 34, pp. 76–81.

Kovalenker, V.A., Pokrovskii, B.G., and Chernyshev, I.V., Isotopic Composition of Hydrogen and Oxygen in Sericites of Paleozoic Epithermal Gold: Primary Data, *Dokl. Akad. Nauk*, 1994, vol. 337, no. 2, pp. 239–242.

Kovalenker, V.A., Safonov, Yu.G., Naumov, V.B., and Rusinov, V.L., The Kochbulak Epithermal Gold–Telluride Deposit (Uzbekistan), *Geol. Rudn. Mestorozhd.*, 1997, vol. 39, no. 2, pp. 127–152.

Kovalenker, V.A., Troneva, N.V., Kuz'mina, O.V., Vyal'sov, L.N., and Goloshchukov, P.M., The First Finding of Kostovite in the Soviet Union, *Dokl. Akad. Nauk SSSR*, 1979, vol. 247, no. 5, pp. 564–569.

Kovalenker, V.A., Evstigneeva, T.L., Malov, V.S., Trubkin, N.V., Gorshkov, A.I., and Heinke, V.R., Nekrasovite, $Cu_{26}V_2Sn_6S_{32}$, as a New Mineral of the Colusite Group, *Mineral. Zh.*, 1984, no. 2, pp. 88–97.

Matsuhisa, Y., Goldsmith, J.R., and Clayton, R.N., Oxygen Isotopic Fractionation in the System Quartz–Albite–Anorthite–Water, *Geochim. Cosmochim. Acta*, 1979, vol. 43, pp. 1131–1140.

Nelson, C.E. and Giles, D.L., Hydrothermal Eruption Mechanism and Hot Spring Gold Deposits, *Econ. Geol.*, 1985, vol. 80, no. 6, pp. 1633–1639.

Nosik, L.P., *Izotopnye metody pri izuchenii mineraloobrazovaniya* (Isotopic Methods in Studying Mineral Formation), Moscow: Nauka, 1986.

Ohmoto, H., Systematics of Sulfur and Carbon Isotopes in Hydrothermal Ore Deposits, *Econ. Geol.*, 1972, vol. 67, pp. 551–578.

Ohmoto, H., Stable Isotope Geochemistry of Ore Deposits, *Rev. Mineral.*, 1986, vol. 16, pp. 491–559.

Ohmoto, H. and Rye, R.O., Hydrogen and Oxygen Isotope Composition of Fluid Inclusion in the Kuroko Deposits, *Econ. Geol.*, 1974, vol. 69, pp. 947–953.

Ohmoto, H. and Rye, R.O., Isotopes of Sulfur and Carbon, *Geochemistry of Hydrothermal Ore Deposits*, New York: Wiley Interscience, 1979, pp. 509–567.

Plotinskaya, O.Yu. and Kovalenker, V.A., The Kairagach Epithermal Gold–Telluride Deposit: Mineralogical-Geochemical Zonation, *Zolotorudnye mestorozhdeniya Uzbekistana: geologiya i promyshlennye tipy* (Gold-Ore Deposits of Uzbekistan: Geology and Commercial Types), Tashkent: IMR, 1998, pp. 57–60.

Plotinskaya, O.Yu., Kovalenker, V.A., Prokof'ev, V.Yu., and Nosik, L.P., Evolution and Character of Fluid Regime on the Kairagach Gold–Telluride Deposit (the Kuramin Mountains), *Mineraloobrazuyushchie flyuidy i rudogenez* (Mineral-Forming Fluids and Ore Genesis), Tashkent: IGiG Akad. Nauk Respubl. Uzbekistan, 1998, pp. 133–135.

Plotinskaya, O.Yu., Kovalenker, V.A., Prokof'ev, V.Yu., Groznova, E.O., and Nosik, L.P., Formation Conditions of Ores in the Kairagach Epithermal Gold–Telluride Deposit (Uzbekistan): Fluid Inclusions and Stable Isotopes, *Trudy X Mezhdunarodnoi konferentsii po termobarogeokhimii* (Proc. X Int. Conf. on Thermobarochemistry), Aleksandrov: VNIISIMS, 2001, pp. 158–179.

Richards, J.P., Alkalic-Type Epithermal Gold Deposits–A Review, *Magmas, Fluid and Ore Deposits. Mineralogical Assoc. of Canada. Short Course Ser.*, 1995, vol. 23, pp. 367–400.

Roedder, E., Fluid Inclusions, *Rev. Mineral.*, 1984, vol. 12 (Monograph).

Rye, R.O., The Evolution of Magmatic Fluids in the Epithermal Environment. The Stable Isotope Perspective, *Econ. Geol.*, 1993, vol. 88, pp. 733–753.

Shvarov, Y.V., The Software for Equilibrium Modeling of Hydrothermal Processes, *Abstr. of the 2nd Int. Symp. "Thermodynamics of Natural Processes,"* Novosibirsk, 1992, p. 51.

Spiridonov, E.M. and Badalov, A.S., New Sulfoselenotellurides and Sulfoselenides of Bismuth from the Kairagach Volcanic Deposit (Eastern Uzbekistan), *Uzb. Geol. Zh.*, 1983, no. 6, pp. 82–84.

Spiridonov, E.M., Chvileva, T.N., and Badalov, A.S., Antimonous Colusite, $Cu_{26}V_2As_2Sb_2S_{32}$, from the Kairagach Deposit and on the Colusite Varieties, *Dokl. Akad. Nauk SSSR*, 1983, vol. 269, no. 3, pp. 706–712.

Taylor, H.P., Jr., Oxygen and Hydrogen Isotope Relationships in Hydrothermal Mineral Deposits, *Geochemistry of Hydrothermal Ore Deposits*, New York: Wiley Interscience, 1979, pp. 237–277.

Tulyaganov, Kh.T., Yudalevich, E.A., Korzhaev, V.P., Kim, O.I., Yaskovich, V.V., Kozlov, V.V., and Poniklenko, I.A., *Karta magmaticheskikh formatsii Uzbekskoi SSR* (The Map of Magmatic Formation in Uzbek Soviet Socialist Republic), Tashkent: Fan, 1984.

White, N.C. and Hedenquist, J.W., Epithermal Environments and Styles of Mineralization: Variations and Their Causes, and Guidelines for Exploration, *J. Geochem. Explor.*, 1990, vol. 36, pp. 445–474.